Alma Mater Studiorum – Università di Bologna

DOTTORATO DI RICERCA IN

SCIENZE E TECNOLOGIE AGRARIE, AMBIENTALI E ALIMENTARI

Ciclo XXXII

Settore Concorsuale: 07/C1 INGEGNERIA AGRARIA, FORESTALE E DEI BIOSISTEMI

Settore Scientifico Disciplinare: AGR/09 MECCANICA AGRARIA

THE POWER DELIVERY EFFICIENCY OF A MECHANICAL FRONT WHEEL DRIVE TRACTOR. A COMPUTATIONAL AND EXPERIMENTAL STUDY

Presentata da: Ing. Nicolò Regazzi

Coordinatore Dottorato: **Supervisore:**

Prof. Massimiliano Petracci **Prof. Ing. Giovanni Molari**

Esame finale anno 2020

The Power Delivery Efficiency of a Mechanical Front Wheel Drive tractor.

A Computational and Experimental Study

Ing. Nicolò Regazzi

Abstract

The reduction of fuel consumptions and the improvement of the efficiency of agricultural vehicles are themes that in the very last few decades have attracted investments and attention from the industrial and scientific community; in this context a study aimed to maximize the efficiency passing through the optimization of the constructive features of an agricultural tractor is certainly suitable. Many studies have been performed for generical off-road vehicles and lunar rover vehicles (L.R.V.) but for agricultural tractors there is still the need to deepen this topic. Agricultural tractors present a very unique powertrain, this means that for the vast majority of cases they are mechanical front wheel drive (M. F. W. D.) and non-isodiametric vehicles. A M.F.W.D. vehicle doesn't use any kind of central differential or transfer case but the torque produced by the engine is splitted between the front and rear axle using a pair of meshing gears. In this thesis the whole driveline has been modeled following a bottom-up approach: starting from the wheel-soil interaction model, passing through the computation of the tractive efficiency of the tractor and arriving to the operating point of the internal combustion engine. The complexity of the implemented model has made necessary an experimental validation that has been carried out by means of several drawbar tests with tractors belonging to different power-classes and on different soils. The correlation between simulations and experimental data was satisfactory (on average $R^2 > 0.72$) thus ensuring the reliability of the model.

Subsequently five constructive parameters: mass distribution, wheels' radius ratio, wheelbase, drawbar height and front wheels' lead have been assumed as the objective of the study and varied on eight levels for a total of 32768 simulations, for each simulation the power delivery efficiency has been evaluated; afterwards by means of a gradient method based on the central difference scheme allowed the estimation of the three most influential parameters. The three most influential parameters are: mass distribution, wheels' radius ratio and front wheels' lead; afterwards these three parameters, by means of the least square method, have been used as indipendent variables of a reduced regression mathematical model (a second order polynomial expression). The first derivative of the reduced model, subsequently set equal to zero, provides the expression of the optimal mass distribution. The study conducted showed that the best configuration is an isodiametric vehicle with the mass distribution slightly shifted towards the front axle and no lead on the front wheels, moreover traditional non-isodiametric tractors have proved to be less efficient than the isodiametric ones and having the optimal mass distribution markedly shifted towards the rear axle.

"The straights? Those boring traits that joint two curves"
Stirling Moss

Declaration

I hereby declare that the following thesis is the result of my Ph.D. research carried out during a period of three years. Contributions from other authors have been appropriately cited and reported in the bibliography. This dissertation is original and has not been submitted to any other institution or university for the achievement of other qualifications/degree.

Nicolò Regazzi

Bologna, October 2019

Acknowledgements

Before leaving the stage to science, I want to take few lines to thank some key people without whom this work was not possible:
First of all my family and my girlfriend for their support and understanding during these years.
Professors Giovanni Molari and Stefan Böttinger for having opened the doors of their institutes and making me passionate about the world of agricultural engineering, agricultural machineries and off-road vehicles.
Mirko Maraldi and Michele Mattetti for constant supervision and support during my studies.
My office mates, Francesco Motti and Enrico Michielan, the so called "Firefighters" for moments of hilarity and pleasant work spent together on the testing track of Cadriano.

Contents

1 Introduction **13**
- 1.1 Problem description . . . 13
- 1.2 The power delivery efficiency in agricultural tractors . . . 14
- 1.3 Literature review . . . 15
  - 1.3.1 Tire/Soil interaction models . . . 16
  - 1.3.2 Experimental studies . . . 28

2 Materials and Methods **29**
- 2.1 The tractor model . . . 29
  - 2.1.1 Equilibrium of the tractor chassis and the driveline model . . . 29
  - 2.1.2 Equilibrium of the wheels and tire-soil interaction model . . . 32
  - 2.1.3 The derivation of the power delivery efficiency . . . 35
  - 2.1.4 The solution algorithm procedure . . . 38
- 2.2 Gradient based method for the analysis of the influence of the tractor design parameters on the power delivery efficiency . . . 39
- 2.3 Simplified regression surfaces based on simulations results . . . 42
- 2.4 Experimental model validation . . . 42
  - 2.4.1 Drawbar tests in open-field conditions . . . 42

3 Results and Discussion **46**
- 3.1 Model Validation . . . 46
  - 3.1.1 Drawbar tests in open field conditions . . . 47
- 3.2 Torque Distribution Factor K_T . . . 51
- 3.3 Gradient Method . . . 52
  - 3.3.1 Optimal layout of the tractor . . . 52

4 Conclusions **62**

List of Figures

1.1 Typical steering mechanism of an agricultural tractor, looking at the front wheels clearly appears that they run on a wider trajectory . . . 14
1.2 Typical trend for: Transmission efficiency η_{TR}, Slip efficiency η_S, Motion efficiency η_M and Power Delivery efficiency η_T 15
1.3 Typical losses occuring along the power delivery process 16
1.4 Typical trend of the Net Traction Ratio/Slip (κ/σ) and Rolling Resistance Coefficient/Slip behavior (ρ/σ) 22
1.5 Bevameter mounted on an off-road vehicle during a soil characterization campaign [36]. 27

2.2 Linear relationship between the slip of the front and rear axle 32
2.3 Simplified scheme of a MFWD driveline from a top view perspective . 33
2.4 Forces, torques, normal and tangential stress distributions at the wheel-soil interface 33
2.5 Efficiencies plot concerning a medium row crop agricultural tractor running on a deformable soil 38
2.6 Drawbar tests in open-field conditions, is clearly visible the front pulling tractor (Case IH Maxxum 115) and the rear braking tractor (New Holland T7-260) 43
2.7 Detail of the load cell used for drawbar force measurements 44
2.9 Rear view of pulling/braking tractors ensemble, is clearly visible the rear mounted plough 45

3.1 Model validation concerning a MFWD row-crop tractor running on a **tilled clayey loam** soil 47
3.2 Model validation concerning a MFWD row-crop tractor running on a **tilled loam** soil 47
3.3 Model validation concerning a MFWD row-crop tractor running on an **untilled loam** soil 48
3.4 Model validation concerning a MFWD row-crop tractor with the 56.31% of the mass acting on the front axle while is running on a light-tilled loam soil 49
3.5 Model validation concerning a MFWD row-crop tractor with the 58.76% of the mass acting on the front axle while is running on a light-tilled loam soil 49
3.6 Model validation concerning a MFWD row-crop tractor with the 32.46% of the mass acting on the front axle while is running on a light-tilled loam soil 50

3.7 Typical trend of the torque distribution factor K_T, computed on a simulative basis 51

3.8 Direction cosines of the gradient of the power delivery efficiency (a), the slip efficiency (b) and the motion efficiency (c) with respect to the scaled variable parameters. Each direction cosine refers to a tractor design parameter among those under investigation. For each plot, the vertical bar encloses the values of the direction cosines of the gradient calculated for all the simulations performed. 53

3.9 Three-dimensional representation of the influence of K_M, L and K_W on $\hat{\eta_T}$, $\hat{\eta_M}$ and on $\hat{\eta_S}$ 54

3.10 Heatmaps of the power delivery efficiency $\hat{\eta_T}$ coming from the regression equations as a function of L, K_M and K_W; the subplot on the left handside corresponds to a value of front-to-rear ratio of kinetic rolling radii K_W equal to 0.70 while the subplot on the right handside to a value of K_W equal to 0.74. 56

3.11 Heatmaps of the power delivery efficiency $\hat{\eta_T}$ coming from the regression equations as a function of L, K_M and K_W; the subplot on the left handside corresponds to a value of front-to-rear ratio of kinetic rolling radii K_W equal to 0.79 while the subplot on the right handside to a value of K_W equal to 0.83. 56

3.12 Heatmaps of the power delivery efficiency $\hat{\eta_T}$ coming from the regression equations as a function of L, K_M and K_W; the subplot on the left handside corresponds to a value of front-to-rear ratio of kinetic rolling radii K_W equal to 0.87 while the subplot on the right handside to a value of K_W equal to 0.91. 57

3.13 Heatmaps of the power delivery efficiency $\hat{\eta_T}$ coming from the regression equations as a function of L, K_M and K_W; the subplot on the left handside corresponds to a value of front-to-rear ratio of kinetic rolling radii K_W equal to 0.96 while the subplot on the right handside to a value of K_W equal to 1.00. 57

3.14 Heatmaps of the motion efficiency $\hat{\eta_M}$ coming from the regression equations as a function of L, K_M and K_W; the subplot on the left handside corresponds to a value of front-to-rear ratio of kinetic rolling radii K_W equal to 0.70 while the subplot on the right handside to a value of K_W equal to 0.74. 58

3.15 Heatmaps of the motion efficiency $\hat{\eta_M}$ coming from the regression equations as a function of L, K_M and K_W; the subplot on the left handside corresponds to a value of front-to-rear ratio of kinetic rolling radii K_W equal to 0.79 while the subplot on the right handside to a value of K_W equal to 0.83. 58

3.16 Heatmaps of the motion efficiency $\hat{\eta_M}$ coming from the regression equations as a function of L, K_M and K_W; the subplot on the left handside corresponds to a value of front-to-rear ratio of kinetic rolling radii K_W equal to 0.87 while the subplot on the right handside to a value of K_W equal to 0.91. 59

3.17 Heatmaps of the motion efficiency $\hat{\eta_M}$ coming from the regression equations as a function of L, K_M and K_W; the subplot on the left handside corresponds to a value of front-to-rear ratio of kinetic rolling radii K_W equal to 0.96 while the subplot on the right handside to a value of K_W equal to 1.00. 59
3.18 Heatmaps of the slip efficiency $\hat{\eta_S}$ coming from the regression equations as a function of L, K_M and K_W; the subplot on the left handside corresponds to a value of front-to-rear ratio of kinetic rolling radii K_W equal to 0.70 while the subplot on the right handside to a value of K_W equal to 0.74. 60
3.19 Heatmaps of the slip efficiency $\hat{\eta_S}$ coming from the regression equations as a function of L, K_M and K_W; the subplot on the left handside corresponds to a value of front-to-rear ratio of kinetic rolling radii K_W equal to 0.79 while the subplot on the right handside to a value of K_W equal to 0.83. 60
3.20 Heatmaps of the slip efficiency $\hat{\eta_S}$ coming from the regression equations as a function of L, K_M and K_W; the subplot on the left handside corresponds to a value of front-to-rear ratio of kinetic rolling radii K_W equal to 0.87 while the subplot on the right handside to a value of K_W equal to 0.91. 61
3.21 Heatmaps of the slip efficiency $\hat{\eta_S}$ coming from the regression equations as a function of L, K_M and K_W; the subplot on the left handside corresponds to a value of front-to-rear ratio of kinetic rolling radii K_W equal to 0.96 while the subplot on the right handside to a value of K_W equal to 1.00. 61

List of Tables

2.1 LETE sand soil parameters 39
2.2 Row crop tractor parameters in the standard configuration 40
2.3 Tractor parameters used in the parametric analysis 40
2.4 Tractor parameters used in the open field validation concerning a Case IH Maxxum 115 43
2.5 Tractor parameters used in the open field validation concerning a New Holland T7-260 44

3.1 Mechanical properties of different soils and transmission efficiency η_{tr} 47
3.2 Fitting accuracy of the model on different soils, evaluated through the coefficient of determination R^2 48
3.3 Values concerning the soil properties and the transmission efficiency η_{tr} for the validation performed with different tractor's mass distributions 48
3.4 Fitting accuracy of the model concerning a tractor with different mass distribution, evaluated through the coefficient of determination R^2 . . 49
3.5 Values of the α_n coefficient concerning the efficiencies regression models 53
3.6 Fitting accuracy of the regression surfaces 54

List of symbols

Symbol	Description	Unit of measure
B	Tractor wheelbase	m
b_f	Width of the contact surface between soil and front tyre	m
b_r	Width of the contact surface between soil and rear tyre	m
c_1	Coefficient for relative position of maximum radial stress	$-$
c_2	Coefficient for relative position of maximum radial stress	$-$
c_3	Coefficient for rut recovery angle location	$-$
c_f	Soil cohesion at the front tyre	Pa
c_r	Soil cohesion at the rear tyre	Pa
F_{DP}	Drawbar pull	N
H_f	Longitudinal force on front axle	N
H_r	Longitudinal force on rear axle	N
h	Drawbar height	m
$j_{0,f}$	Shearing deformation modulus at the front tyre	m
$j_{0,r}$	Shearing deformation modulus at the rear tyre	m
j_f	Shear displacement at the front tyre	m
j_r	Shear displacement at the rear tyre	m
K_M	Static mass distribution ratio	$-$
K_P	Pull distribution ratio	$-$
K_W	Front to rear ration of kinetic rolling radii	$-$
$k_{c,f}$	Parameter related to soil cohesion at the front tyre	$N \cdot m^{-n-1}$
$k_{c,r}$	Parameter related to soil cohesion at the front tyre	$N \cdot m^{-n-1}$
$k_{\phi,f}$	Parameter related to soil internal friction angle at the front tyre	$N \cdot m^{-n-2}$
$k_{\phi,r}$	Parameter related to soil internal friction angle at the rear tyre	$N \cdot m^{-n-2}$
L	Front wheels lead	$-$
l_1	Longitudinal distance between front axle and centre of gravity	m
l_2	Longitudinal distance between rear axle and centre of gravity	m
M_e	Engine torque at the flywheel	$N \cdot m$
M_f	Torque at the front axle	$N \cdot m$
M_r	Torque at the rear axle	$N \cdot m$
M_{tr}	Torque at the output shaft of the transmission	$N \cdot m$
n	Bekker sinkage exponent	$-$
r_f	Front tyre kinetic rolling radius	m
r_r	Rear tyre kinetic rolling radius	m
s_f	Front wheel slip	$-$
s_r	Rear wheel slip	$-$

Symbol	Description	Unit of measure
V_f	Vertical load on front axle	N
V_r	Vertical load on rear axle	N
v	Tractor speed	$m \cdot s^{-1}$
W	Tractor weight	N
β_i	$i-th$ coefficient of the regression function	$various$
ϕ	Soil internal friction angle	rad
η_M	Motion efficiency	$-$
η_S	Slip efficiency	$-$
η_T	Power delivery efficiency	$-$
η_{tr}	Transmission efficiency	$-$
$\eta_{tractive}$	Tractive efficiency	$-$
θ	Variable of integrations for the stress functions	rad
$\theta_{1,f}$	Front wheel entry angle	rad
$\theta_{1,r}$	Rear wheel entry angle	rad
$\theta_{2,f}$	Front wheel rut recovery angle	rad
$\theta_{2,r}$	Rear wheel rut recovery angle	rad
$\theta_{m,f}$	Front wheel angle of maximum stress	rad
$\theta_{m,r}$	Rear wheel angle of maximum stress	rad
σ_f	Front wheel normal stress	MPa
σ_r	Rear wheel normal stress	MPa
τ_d	Transmission front axle lead ratio	$-$
τ_f	Front wheel tangential stress	MPa
τ_r	Rear wheel tangential stress	MPa
τ_{tr}	Transmission gear ratio	$-$
ω_e	Engine speed	$rad \cdot s^{-1}$
ω_f	Front axle angular velocity	$rad \cdot s^{-1}$
ω_r	Rear axle angular velocity	$rad \cdot s^{-1}$

Outline of the thesis

This doctoral thesis comes from a 3-years study summarized in an article called: "A theoretical study of the parameters affecting the power delivery efficiency of an agricultural tractors" published in Biosystems Engineering (Regazzi et al. 2019 [26]). This thesis is organized in the following manner:

- INTRODUCTION where some concepts of the traction mechanics are explained; furthermore an extensive review of the state of the art had been carried out, considering different typology of approach.
- MATERIALS AND METHODS where is provided a depth overview of the governing equations of the tractor model, of the testing procedure to validate the model and the methods used for the post-processing of the results.
- RESULTS AND DISCUSSION where it is possible to observe the results coming from the simulations performed and also a comparison between simulated and experimental data in different conditions
- CONCLUSIONS where are reported the conclusions that can be drawn from the study conducted.

Chapter 1

Introduction

1.1 Problem description

The improvement of the efficiency of vehicles and the reduction of fuel consumptions is something that have attracted the attention of the researchers and of off-highway vehicles manufacturers [14].
The ability to build vehicles with an high efficiency level pass through the ability to predict the behavior under operational condition, to achieve this goal different paths can be assumed, ranging from purely experimental to purely computational: in this thesis we used a computational/simulative approach followed by an experimental validation; the reason that lays behind this kind of choice is that is possible to vary by a large amount all the dimensional features of a tractor overcoming the typical experimental limits.
The field of off-highway vehicles is very broad covering different building architecture, for this thesis a particular kind of 4WD wheeled agricultural tractor have been considered, the so called mechanical front wheel drive (M.F.W.D.), which represents the consolidated state of the art for the driveline of a tractor. For this type of driveline, the studies found in the literature, were not completely satisfactory. This kind of architecture, when operating in 4WD mode, doesn't use any kind of central differential or transfer case but just a pair of meshing gears located on the output shaft of the gearbox.
A M.F.W.D. transmission is characterized by pros and cons: from the positive side we underline the possibility to freely variate the torque distribution between the axles and the overcoming of the open differential behavior, avoiding that torque completely flows to the purely slipping axle; the negative aspects are related to the steering mechanism, in fact the front wheels run on a longer trajectory thus requiring an higher tangential speed, the so-called front wheels' lead, that deteriorate the power delivery efficiency. This kind of constructive architecture can be also very dangerous for vehicle transmission due to torsional windup phenomena that may occur at low slippage value. Torsional windup happens when torque is applied and the rotation of one end of a shaft is greater than the one on the other end.
As appears from the previous lines the problem of the improvement of the efficiency for off-road/agricultural vehicles is very hard to solve due to the mechanical complexity of the system involved, however the study conducted, appropriately supported by experimental evidences, has made possible some clarifications on the constructive features affecting the power delivery efficiency.

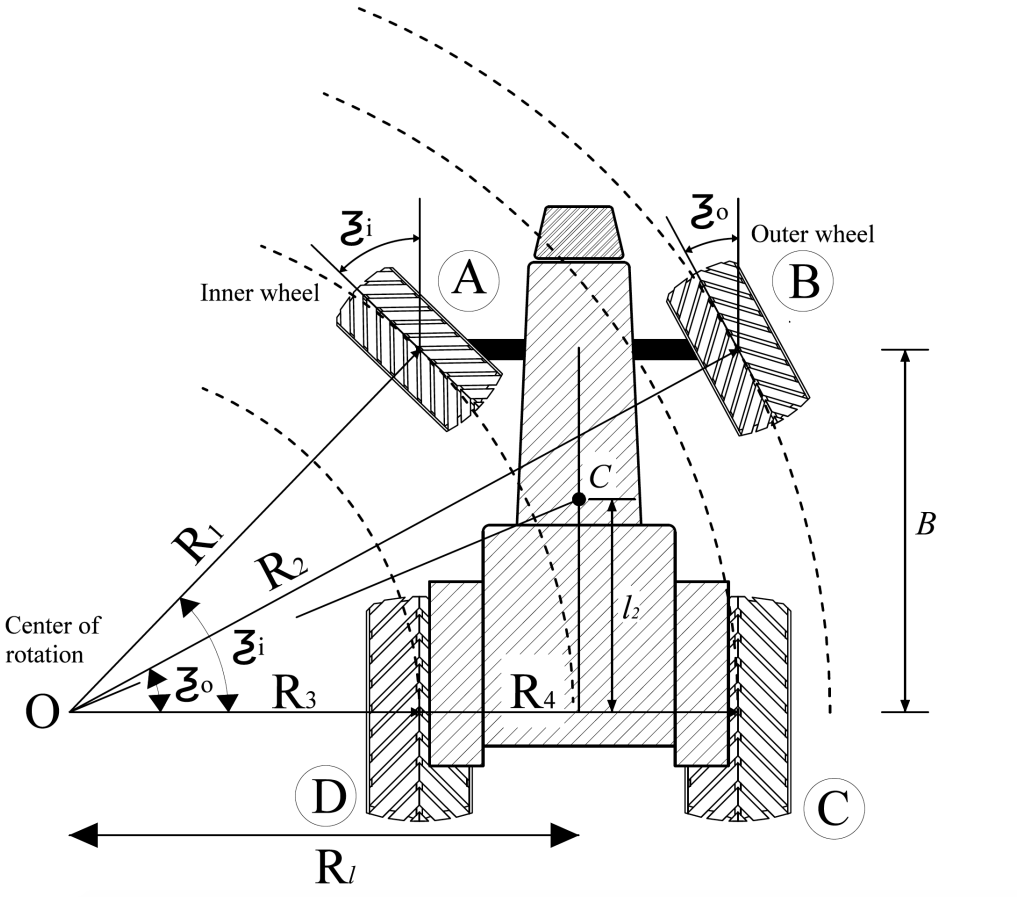

Figure 1.1: Typical steering mechanism of an agricultural tractor, looking at the front wheels clearly appears that they run on a wider trajectory

1.2 The power delivery efficiency in agricultural tractors

In agricultural tractors the power generated by the internal combustion engine flows down the driveline passing the gearbox, the MFWD system, the differentials, the epicycloidal reducer and finally through the tires transformed into net power, obviously the power given by the engine is not equal to the net power produced by the vehicle, this process is called "Power Delivery" and along this stream many power losses occur, thus, to account this kind of phenomena we have to insert an efficiency factor called "Power Delivery Efficiency" η_T, this factor is not constant but can vary a lot depending on the operational conditions of the vehicle and on the amount of drawbar force required by the implement. In the field of agricultural tractors, to maximize the power delivery efficiency is a well known practice to set the drawbar force in order to have a slip of the vehicle in the range of 10%-15%.
The power delivery efficiency is defined as the power delivered by the vehicle divided by the power provided by the engine but can be also computed as the product of three different efficiencies:

- η_{TR}: the **transmission efficiency** that accounts all the losses occurred along the tractor powertrain and is defined as the ratio between the power at the outer shaft of the gearbox and the power delivered by the engine

- η_S: the **slip efficiency** that accounts for the difference between the theoretical and the actual speed of the vehicle and is defined as the ratio of the actual power at the wheels and the theoretical power at the wheels
- η_M: the **motion efficiency** that accounts for the rolling resistance and is defined as the efficiency factor that consider the power losses occurred in the conversion process from the thrust force at the running wheel to the drawbar force at the hitch.

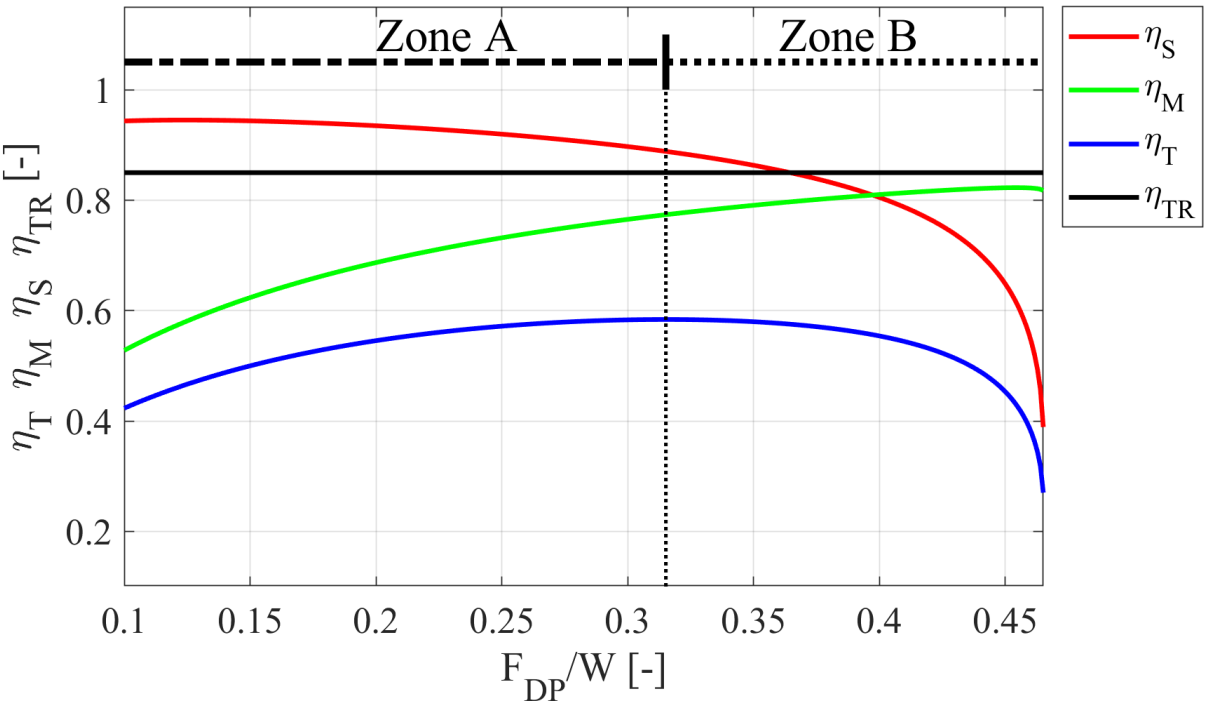

Figure 1.2: Typical trend for: Transmission efficiency η_{TR}, Slip efficiency η_S, Motion efficiency η_M and Power Delivery efficiency η_T

Since agricultural tractors are designed with particular attention to provide drawbar force (F_{DP}) is important to catch the dependancy of all the different type of efficiency from the drawbar force, as is possible to see from Fig. 1.2, the power delivery efficiency (η_T) exhibits a highly non linear behavior with a peak slightly before the intersection of the slip (η_S) and motion (η_M) efficiencies curves, this point is the so-called "Sweet Operating Spot" where the driver should maintain the vehicle during the work. The "Sweet Operating Spot" also identifies two different operational regimes: one governed by the motion efficiency (Zone A) and the other governed by the slip efficiency (Zone B); typically in the Zone A the vehicle is over-ballasted while in the Zone B is under-ballasted thus the easiest way to improve the efficiency is to adjust the weight of the tractor.

1.3 Literature review

The increase of the agricultural/off-road vehicle efficiency is something that attracted the attention of researchers since a long time, in the literature we can see

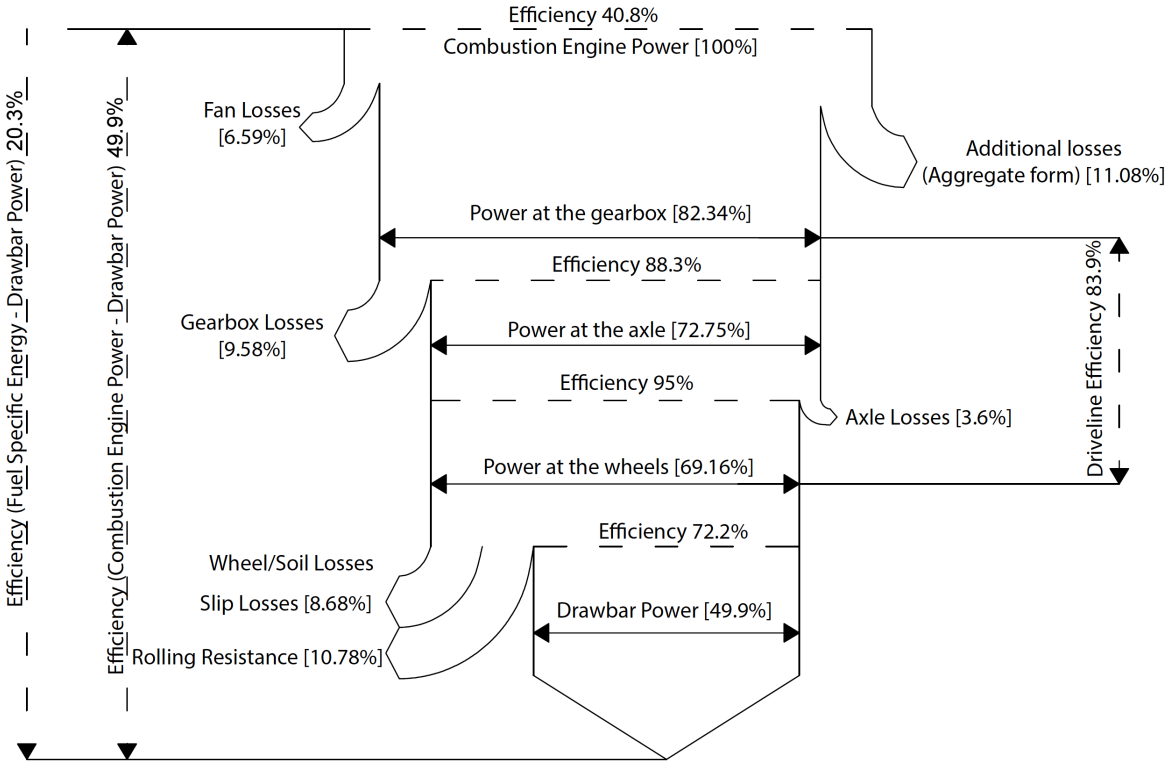

Figure 1.3: Typical losses occuring along the power delivery process

a broad range of models and approaches, many worked only on the modeling of the tire-soil interaction, many other looked at the vehicle as a whole at macro-scale level, in the following lines will be provided an overview of what has been done for off/road agricultural vehicles concerning the tractive performances.

1.3.1 Tire/Soil interaction models

Since many losses in the power delivery process happen at the tire/soil interface the implementation of a wheel-soil interaction model plays a crucial role, the scientific literature provides different model typology: analytical, empirical and semi-empirical models; in the following pages a depth review will be conducted.

Analytical models

This kind of approach is very elegant and ensures a certain level of comprehension of the physical phenomenon. Baladi & Rohani [2] developed a model for the description of the tire-soil interaction based on springs arranged in series and from these was possible to determine the stresses acting on the interface. At the beginning of this century the finite element method (F.E.M.) began to be used, this method is particularly indicated to investigate very complex problems including geometrical and material non linearities. Upadhyaya et al. [30] described the usage of the Finite Element Method for traction related problems in the field of off-road

vehicles. Aubel [1] and Schmid [27] characterized the soil as an elastoplastic material subjected to the Drucker-Prager criterion while the wheel is modeled as three concentric circles with an homogenous and elastic behaviour; these three circles represent the tire carcass, the tire tread and the wheel rim; this model predict the deformation of the soil and of the tire, the contact geometry and the bulldozing effect. Fervers [11] developed a bidimensional FEM model, he substitutes the tire carcass with characteristic force-deformation relationship and the soil was modeled through the Drucker-Prager criterion. Ibuki & Oida [17] used the discrete element method (DEM) for modeling the tire-soil interaction but this kind of approach was very computationally demanding and the simulation time was pretty high for this reason a complete DEM approach was superseded by mixed (FEM/DEM) approach. Nakashima & Oida [24] proposed a mixed FEM/DEM approach, they used the discrete element method to model the soil in contact with the tire and the remaining part of the soil and the wheel with the finite element method. However, despite the mathematical elegance of these models we preferred to discard them for the high computational cost that even in the less demanding versions they would have had, moreover the lack of appropriate constitutive bond and boundary conditions limited a lot the diffusion of these models.

Empirical models

Empirical models have been developed in an initial version during the fifties for military purposes deriving from the need of the U.S. Army, the goal was to understand quickly and easily if a certain place could be crossed by military vehicles and for this reason were more related to the trafficability of the soil instead of the prediction of the tractive performances of the vehicle and were named as "GO/NO GO Models"; this kind of models relies on a soil parameter called "Cone Index" (CI), that represents the penetration resistance given by the soil. The first model that overcomes the "GO/NO GO Models" is the one provided by Freitag [12] and Turnage [32], they developed a model based on empirical coefficients, the so-called "Wheel Numeric Coefficients", these coefficients can be subdivided in two different type: "Clay Numeric" (N_C) and "Sand Numeric" (N_S)

$$N_C = (\frac{CI \cdot b \cdot d}{W}) \cdot (\frac{\delta}{h})^{1/2} \cdot (\frac{1}{1 + b/2d}) \tag{1.1}$$

$$N_S = G \cdot \frac{(b \cdot d)^{3/2}}{W} \cdot \frac{\delta}{h} \tag{1.2}$$

knowing that:

- δ is the tire deflection
- h is the tire section height
- d is the tire diameter
- b is the the section width of the tire
- W is the axle load
- CI is the cone index value

- G is the cone index gradient with the depth

Once the coefficients N_C and N_S have been evaluated they can be inserted in two equations for the evaluation of the tractive performance and of the rolling resistance.

$$\frac{R}{W} = 0.04 + \frac{0.020}{M - 2.5} \tag{1.3}$$

$$\frac{D_{20}}{W} = 0.80 + \frac{1.31}{M - 2.45} \tag{1.4}$$

knowing that:

- R is the rolling resistance
- D_{20} is the drawbar force exerted at 20% of slip
- M is the wheel numeric (e.g. N_C or N_S)

Wismer & Luth [36, 37] introduced a new "Wheel Numeric Coefficient" for cohesive/frictional soil expressed by the following equation:

$$C_n = \frac{CI \cdot b \cdot d}{W} \tag{1.5}$$

However afterward Turnage [32] noticed that for frictional soils the cone index coefficient was not ideal for the description of the tractive behavior of tires and thus he revised the formulation of the "Sand Numeric", the "Sand Numeric" provided by Turnage is independent from the Cone Index value, is indicated with N_{SEY} and is expressed by the following expression

$$N_{SEY} = G_{EY} \cdot \frac{(b \cdot d)^{3/2}}{W} \cdot \frac{\delta}{h} \tag{1.6}$$

knowing that:

- G_{EY} is the sand compactibility

At the beginning of the seventies Wismer & Luth [36, 37] introduced a new empirical model for the evaluation of tractive performance of off-road vehicles equipped with bias-ply tires running on slightly compactable soils

$$\frac{R}{W} = \frac{1.2}{C_n} + 0.04 \tag{1.7}$$

$$\frac{T}{r \cdot W} = 0.75 \cdot (1 - e^{-0.3 \cdot C_n \cdot s}) \tag{1.8}$$

knowing that:

- T is the input torque at the wheel hub
- r is the rolling radius
- s is the tyre slip

The evaluation of the rolling radius is proposed through an empirical formulation as follows:

$$r = \frac{2.5 \cdot UR \cdot LR}{1.5 \cdot UR + LR} \tag{1.9}$$

Subsequently Charles & Schuring [8] proposed a different version of the rolling radius equation to account also for different tyre building technology:

$$r = (1 - K) \cdot UR + K \cdot LR \tag{1.10}$$

knowing that:

- UR is the unloaded radius, the radius of the tyre when no vertical loads are applied
- LR is the loaded radius, the radius of the tyre when vertical loads are applied
- K is a tire dependent factor

The reliability of this model is ensured if the following conditions are satisfied:

- $b/d \approx 0.3$
- $\delta/h \approx 0.2$
- $r/d \approx 0.475$

Later Zoz & Brixius [44] introduced in the scientific community a new empirical-traction model for tires based on empirical tests performed on concrete arriving to the following exponential model:

$$\frac{D}{W} = 1.02 \cdot [1 - e^{-K(\frac{b \cdot d}{W}) \cdot s}] \tag{1.11}$$

$$\frac{T}{r \cdot W} = \frac{D}{W} + 0.02 \tag{1.12}$$

knowing that:

- K is a model specific constant

Observing the Eq. 1.12 is possible to notice that the motion resistance is estimated as 2% of the dynamic axle load

During the eighties Bashford et al. [3] and Byerly et al. [7] proposed a more general model to account also for the tractive efficiency

$$\frac{D}{W} = A \cdot (1 - e^{-B \cdot s}) + C \tag{1.13}$$

$$TE = (1 - s) \cdot [1 - \frac{F}{1 - e^{e \cdot s}}] \tag{1.14}$$

knowing that:

- TE is the tractive efficiency

- D is the drawbar pull
- A, B, C, E, F are soil/tire related constants

The most famous and widely used empirical model is the one developed by Brixius [6] for bias-ply tires:

$$\frac{T}{rW} = 0.88(1 - e^{-0.1 \cdot B_n}) \cdot (1 - e^{-7.5 \cdot s}) + 0.04 \tag{1.15}$$

$$\frac{R}{W} = \frac{1}{B_n} + 0.04 + \frac{0.5 \cdot s}{\sqrt{B_n}} \tag{1.16}$$

$$B_n = (\frac{CI_f \cdot b \cdot d}{W}) \cdot (\frac{1 + 5 \cdot \frac{\delta}{h}}{1 + 3 \cdot \frac{\delta}{h}}) \tag{1.17}$$

$$CI_f = CI_i \cdot (1 + 1.8e^{-0.11 \cdot B_n}) \tag{1.18}$$

knowing that:

- B_n is the mobility number
- CI_f is the after traffic cone index
- CI_i is the cone index of the previous pass

The model defined by Brixius [6] was innovative since it introduced two interesting novelties: the first one is the accounting of the multipass effect through the Eq. 1.18, the second one is to relate the rolling resistance with the slip accounting also for the slip-sinkage phenomenon.
Afterward, Evans et al. [9, 10] slightly modified the model developed by Brixius in order to adapt to M. F. W. D. vehicles.

Upadhyaya et al. [34] and Upadhyaya & Wulfsohn [35] proposed a particular empirical model that encapsulates for the first time normal and shear stresses into empirical equations, the shear stresses are formulated through the Mohr-Coulomb criterion and the normal stresses through the Bekker equation [4, 5]. This model relies on several multivariate regression equations and on the evaluation of stresses, shear stresses can be evaluated by means of the direct shear apparatus and normal stresses using a bevameter.

$$\frac{D}{W} = a(1 - e^{-c \cdot S}) \tag{1.19}$$

$$\frac{T}{rW} = a'(1 - b^{-c' \cdot S}) \tag{1.20}$$

but the coefficients a' and a are computed through the multiple linear regressions

$$aW = 1.73 + 0.572\tau_{max}A_c + 3.589\tau_{max} \cdot K \cdot l_w + 5.672\frac{p}{K_r} \tag{1.21}$$

$$acW = 0.881(\frac{\delta_t - \delta_s}{l_c})^{0.183}(\frac{\delta_t}{l_c})^{1.346}(\frac{l_w}{K})^{-1.717}(\frac{l_c}{K})^{-1.743}(\frac{l_c l_w}{A_c})^{4.198}(\tau_{max}A_c)^{0.685} \tag{1.22}$$

$$a'W = 5.843 - 3.697(\frac{aWK}{l_c}) + 11.778(\frac{aW^2}{294.1l_c}) \tag{1.23}$$

$$a'b = 0.053 + 0.865a' - 1.488x_1 + 13.496x_1^2 \tag{1.24}$$

$$a' = 0.878a + 0.197 \tag{1.25}$$

$$b = 0.91 \tag{1.26}$$

Knowing that the variables used are listed below:

- A_c is the tyre/soil contact patch $[m^2]$
- τ_{max} is the maximum shear stress defined through the Mohr-Coulomb criterion
- l_w contact width [m]
- K is the shear modulus [m]
- K_t is the tyre stiffness in the tangential direction [kN/m]
- K_r is the Reece sinkage coefficient
- p is the average contact pressure W/A_c
- l_c is the contact length m
- $x_1 = \frac{\delta_t}{l_c}$
- $x_2 = \frac{\delta_s}{n+1}/l_c$
- δ_s = maximum soil deformation [m]
- δ_t = total deformation (soil+tire) in the vertical direction [m]
- n = exponent introduced by Bekker

Schreiber [28] introduced an empirical model for the evaluation of tractive performance, this model is able to predict the curves concerning the Net Traction Ratio[1]/Slip[2] and Rolling Resistance Coefficient[3]/Slip behaviour and is based on six adimensional K factors related both with the soil and the tyre; these six K factors vary between 0 and 1 and are:

- K_{tyre} is a coefficients that accounts for the tyre features, especially for the radius, the width and the inflation pressure
- K_{cover} is a coefficient that accounts for the soil cover depending on the presence of stubble, grass, etc...

[1]Is the ratio between the traction force and the vertical force acting on the wheel

[2]The slip σ is defined as: $\sigma = 1 - \frac{V}{V_t}$, where V is the actual speed of the tractor and V_t is theoretical speed of the tractor

[3]Is the ratio between the rolling resistance force and the vertical force acting on the wheel

- $K_{strength,A}$ is a coefficient that accounts for the mechanical strength of the first soil layer
- $K_{strength,B}$ is a coefficient that accounts for the mechanical strength of the second soil layer
- K_{clay} is a coefficient that accounts for the clay content of the soil
- $K_{moisture}$ is a coefficient that accounts for the moisture content of the soil

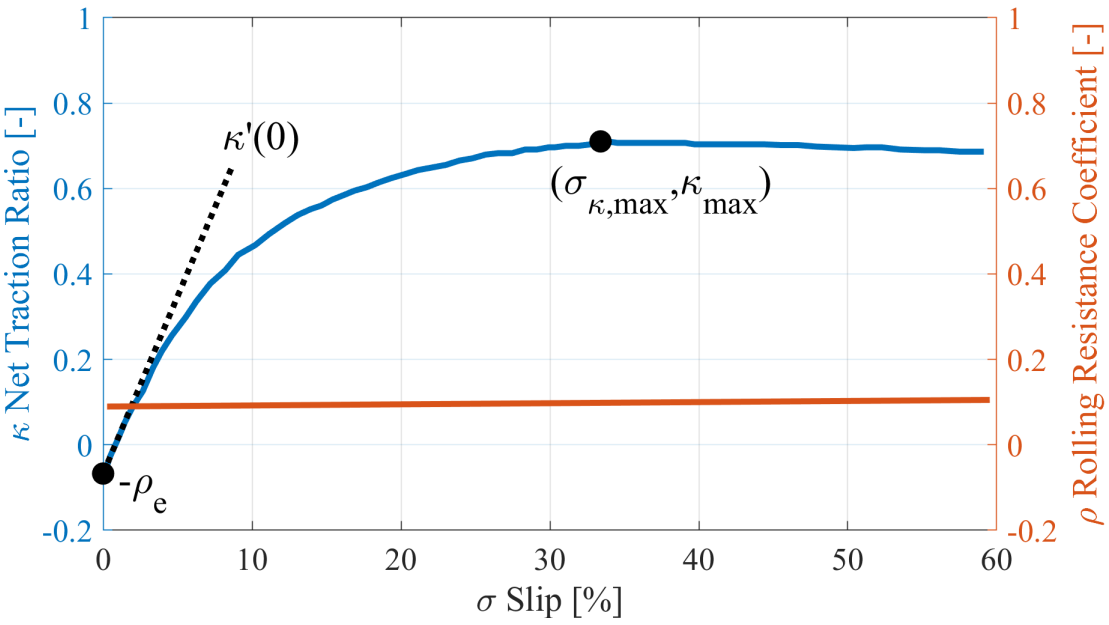

Figure 1.4: Typical trend of the Net Traction Ratio/Slip (κ/σ) and Rolling Resistance Coefficient/Slip behavior (ρ/σ)

The Net Traction Ratio/Slip and Rolling Resistance/Slip curves are fully described by four elements as is possible to see in the Fig. 1.4:

- κ_{max} is the maximum value of the Net Traction Ratio
- $\sigma_{\kappa_{max}}$ is the slip where the Net Traction Ratio peaks
- $\kappa'(0)$ is the slope of the initial branch of the Net Traction Ratio/Slip curve
- $-\rho_e$ is the initial value for the external Rolling Resistance Coefficient

The two curves can be mathematically expressed by the following two mathematical equations:

$$\kappa = a_1 - b_1 \cdot e^{-c_1 \cdot \sigma} - d_1 \cdot \sigma \tag{1.27}$$

$$\rho = a_2 + b_2 \cdot \sigma \tag{1.28}$$

The coefficients a_1, b_1, c_1, d_1 and a_2, b_2 can be computed through the following procedure:

$$\kappa_{max} = 0.31 + 0.13K_{cover} + 0.11K_{strength,A} + 0.09K_{strength,B} + \tag{1.29}$$

$$+0.07K_{clay} + 0.09(-4K^2_{moisture} + 4K_{moisture})$$

$$\sigma_{\kappa_{max}} = 0.55 + 0.18K_{cover} + 0.12K_{strength,A} + \tag{1.30}$$

$$+0.08K_{strength,B} + 0.06K_{clay} + 0.08K_{moisture}$$

$$\kappa'(0) = 5 + 2.8K_{cover} + 1.3K_{strength,A} \tag{1.31}$$

$$\rho(\sigma = 0) = 0.18 + 0.02K_{cover} - 0.06K_{strength,A} - 0.05K_{strength,B} + \tag{1.32}$$

$$+(K_{strength,A} + K_{strength,B} - 2) \cdot 0.03K_{tyre}$$

$$\rho_e = \rho - \rho_i \tag{1.33}$$

Where ρ_i is the internal rolling resistance and is computed as:

$$\rho_i = 0.015 + 0.01 \cdot K_{tyre} \tag{1.34}$$

Then is possible to introduce a standardised slope for the curve at initial point

$$\kappa'_{sta}(0) = \frac{(u-1) \cdot ln(u)}{1 + u \cdot (ln(u) - 1)} \tag{1.35}$$

Where u is a supporting variable expressed as below

$$u = e^{\frac{ln(K'_{sta}(0))}{-0.194}} \tag{1.36}$$

$$b_1 = \frac{\kappa_{max} + \rho_e}{1 - u \cdot (1 - ln(u))} \tag{1.37}$$

$$c_1 = -\frac{ln(u)}{\sigma_{\kappa_{max}}} \tag{1.38}$$

$$d_1 = u \cdot b \cdot c \tag{1.39}$$

$$a_1 = b_1 - \rho_e \tag{1.40}$$

$$a_2 = -\rho_e \tag{1.41}$$

$$b_2 = 0.013 \tag{1.42}$$

However this model is not completely suitable to describe the behavior of current tires since it was calibrated on a huge number of measurements performed during the eighties but for bias-ply tires, nowadays the vast majority of tractors are fitted with radial tires thus it tends to underestimate the tractive performances and also the dependency from the tyre inflation pressure and the deterioration of the tractive performance due to the wear are not completely modeled, for these reasons to adapt the model to the current demand several correction factors are required. The model as appears in the final form is reported below.

The β_i correction factors used in the conversion process into a radial tire model are five and affects Eqs. 1.29, 1.30 and 1.31:

$$\kappa_{max} = 0.31 + 0.13K_{cover} + 0.11K_{strength,A} + 0.09K_{strength,B} + \tag{1.43}$$

$$+0.07K_{clay} + 0.09(-4K^2_{moisture} + 4K_{moisture}) + \beta_1 K_{tyre} + \beta_2 K_{wear}$$

The mathematical task of the β_1 coefficient is to increase the value of the maximum traction force produced by the vehicle according to the fact that radial tires exhibit better tractive performance.

The mathematical task of the β_2 coefficient is to decrease the maximum traction force that can be produced by the tire proportionally with the wear of the tire.

$$\sigma_{\kappa_{max}} = \beta_3 + 0.18K_{cover} + 0.12K_{strength,A} + \tag{1.44}$$

$$+0.08K_{strength,B} + 0.06K_{clay} + 0.08K_{moisture}$$

The mathematical task of the β_3 coefficient is to move forward the value at which the traction force peaks.

$$\kappa'(0) = 5 + 2.8K_{cover} + 1.3K_{strength,A} + \beta_4 K_{pressure} + \beta_5 K_{wear} \tag{1.45}$$

The mathematical task of the β_4 coefficient is to decrease the slope of the first part of the traction curve accordingly with the tyre inflation pressure, in order to model the fact that for the same traction force exerted a tire inflated at lower pressure tends to slip less.

The mathematical task of the β_5 coefficient is to increase the slope of the first part of the traction curve accordingly with the wear of the tyre, in order to model the fact that a tire with an high degree of wear tends to slip more.

The values of the β_1, β_2, β_3, β_4 and β_5 are reported in the table below and had been estimated through the least square method, based on experimental trials:

Correction coefficient	Value [-]
β_1	0.22
β_2	0.03
β_3	62.50
β_4	-1.82
β_5	0.50

The mathematical simplicity and the dependence on just one soil parameter make the empirical models particularly suitable to predict the tractive performances of

agricultural tractors but as highlighted by Wong [40, 41] they are not so reliable when the testing conditions are far from the conditions used during the calibration of the coefficient, moreover this kind of models are limited to the prediction of the traction-slip relationship and the motion resistance but they do not provide any further details on the underlying mechanics of the vehicle and for this reason we preferred to discard this kind of models.

Semi-empirical models

Semi-empirical models are those models that describe the wheel-soil interaction through the usage of a device called bevameter [4, 5, 40, 41]. A generic vehicle, operating in off-road conditions, tends to stress the soil by transferring normal and shear loads: the bevameter is an experimental device that tends to simulate this physical phenomenon by means of two different tests. The first one is the plate penetration test, useful for the characterization of the pressure-sinkage relationship; the second one is the shear stress test, useful for the characterization of the shear stress-shear displacement relationship. These semi-empirical models rely on two fundamental assumptions concerning the deformation of the soil:

- the vertical deformation of the soil under the weight of a wheel is assumed analogous to those provided by a plate sinking into the soil
- the shear deformation of the soil is assumed similar to those produced by a plate to which a torque is applied

Vertical and shear deformations are generated by normal and shear stresses:

Normal stresses under the plate are defined in accordance with the Bekker theory [4,5] in the following manner:

$$\sigma = (\frac{K_c}{b} + K_\phi)z^n \tag{1.46}$$

knowing that:

- K_c is a cohesion related parameter
- K_ϕ is the internal friction angle parameter
- b is the width of the sinking plate comparable to tire width
- z is the sinkage
- n is an empirical coefficient called "Bekker exponent"

Shear stresses are defined through the Janosi-Hanamoto theory [19], that proposed a modified version of the Mohr-Coulomb equation

$$\tau = (c + \sigma \cdot tan\phi) \cdot (1 - e^{\frac{j}{J_0}}) \tag{1.47}$$

knowing that:

- c is the soil cohesion

- σ are the normal stresses defined by the Bekker equation
- ϕ is the internal friction angle
- j is the shear displacement
- j_0 is the shearing deformation modulus

Thanks to the soil parameters previously outlined is possible to define also the maximum soil deformation and the motion resistance

$$z_0 = (\frac{p_{gr}}{\frac{K_c}{b} + K_\phi})^{\frac{1}{n}} \tag{1.48}$$

$$MR = \frac{b \cdot p_{gr}^{\frac{n+1}{n}}}{(n+1)(\frac{K_c}{b} + K_\phi)^{\frac{1}{n}}} \tag{1.49}$$

knowing that:

- p_{gr} is the average ground pressure defined as the summation of the pressure due to carcass stiffness and of the inflation pressure
- z_0 is the maximum soil deformation
- MR is the motion resistance, defined as the resistance force encountered by the wheels when trying to move from a stall condition or during an acceleration phase, this kind of resistance must be overcome in order to keep the vehicle in motion.

Bekker [5] introduced in his study the problem of tire deformability by means of a parameter called critical ground pressure p_{gcr} that determines the inflation pressure threshold of rigid tire behavior: beyond this limit the tire behaves as a rigid tire, below as deformable tire; p_{gcr} is defined in the following manner:

$$p_{gcr} = (\frac{K_c}{b} + k_\phi)^{\frac{1}{2n+1}} \cdot (\frac{3W}{(3-n)b\sqrt{D}})^{\frac{2n}{2n+1}} \tag{1.50}$$

knowing that:

- W is the vertical weigth acting on the wheel
- D is the tire diameter

The tire deformability is since many years a great problem to handle and in particular the determination of the rolling radius; many authors (Fujimoto [13], Perdok [25], Wong [35]) suggested to consider the rolling radius of a deformable tire as a rigid tire with a bigger diameter.

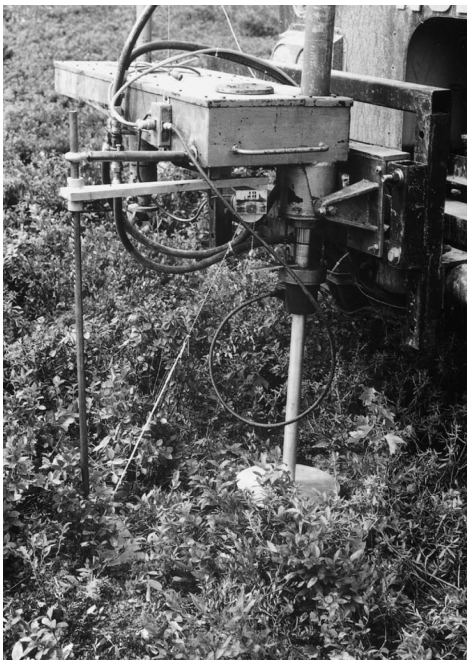

Figure 1.5: Bevameter mounted on an off-road vehicle during a soil characterization campaign [36].

Whole-vehicle model

The formulation of the stresses provided by Bekker [4, 5] and Janosi & Hanamoto [19], as previously outlined, is not very computationally demanding and so was identified as particularly suitable for the development of whole-vehicle computer model, as done by many scientist, for example: Senatore & Sandu [29, 30] and Liang et al. [23]. The development of a whole vehicle model relies in first instance on the modeling of a wheel, the first scientist that developed a wheel model was Wong in the late sixties with two papers concerning towed and driven rigid wheels [42, 43], in these two articles he presented a reconstruction of the forces acting at the wheel hub by means of three integral equations solved through the Simpson numerical integration rule. Senatore & Sandu [29, 30] developed a whole-vehicle dynamic model (including also the tire deformability as a function of the inflation pressure), for the evaluation of the performance of a generic off-road vehicle, the model was characterized by the following features: isodiametric off-road tires and a transfer case that behaves like a central differential; this model was used for both hybrid and internal combustion engine; furthermore it has been validated using an automotive simulation toolbox ($CARsim^{TM}$) as benchmark for the results of the simulations coming from the whole-vehicle model. Liang et al. [23] used a similar approach but for an isodiametric lunar rover vehicle (L. R. V.), in this case a complete validation is missing and the problem was faced just from a theoretical point of view. The vehicle model, object of the study of this doctoral thesis, followed a similar approach using a stress based model, however the model proposed differs from the previous because is referred to a Mechanical Front Wheel Drive (M. F. W. D.) off-road vehicle with non-isodiametric wheels; also the validation procedure was different in fact was carried out through a comparison with purely experimental data. The choice fell on this type of approach because in addition to being relatively computational undemanding allowed a deep comprehension of the underlying mechanics.

1.3.2 Experimental studies

Experimental studies have been conducted for many years, in particular a great effort was spent to clarify the influence of mass distribution, tire inflation pressure and tire dimensions, the underlying reason is that these three parameters are those that can be easily modified by the user during in-field operations. Bashford [3] studied the influence of mass distribution and the front wheels lead on the power delivery efficiency for a tractor operating in M. F. W. D. mode, he varied the lead of the front wheels in different steps ranging from -0.03 to 0.13 and then provided optimal values for mass distribution; Bashford varied the mass distribution through the variation of the position of the ballast and the front wheels lead through the variation of the tire dimensions. Janulevicious et al. [20, 21] studied how the inflation pressure affects the front wheels lead and suggested an optimal inflation pressure in order to provide good tractive performances. In a similar framework Stoilov & Kostadinov [31] studied the influence of the mass distribution on the slip efficiency for a four-wheel drive forestry skidder, he measured the forces acting on the wheel hub and the slip by means of wheel force transducers and phonic wheels for different mass distribution observing that a mass distribution shifted toward the front axle improves the slip efficiency of the vehicle These kind of approach is very practical and allows immediately to derive some conclusions but have also some disadvantages: is very difficult to decouple the influence of a parameter from the others, for example the variation of the inflation pressure implies also the variation of the tire dimensions and the front wheels lead making the comprehension of the physical phenomenon very difficult.

Chapter 2

Materials and Methods

2.1 The tractor model

As previously outlined, this study is, in first instance, composed by the development of a whole tractor model; the model considers a non-isodiametric, Mechanical Front Wheel Drive vehicle which represents the most common architecture for commercial tractors. The model relies on a bottom-up and semi-empirical approach: bottom-up because it starts from the stresses at the wheel-soil interface and through the gearbox arrive at the internal combustion engine, semi-empirical because not all the parameters used in the model are physically sound. Furthermore, semi-empirical methods are simpler and not very computational demanding but still provide some insights on the underlying mechanics.

2.1.1 Equilibrium of the tractor chassis and the driveline model

Tractors are vehicles that during in-field operational conditions (Fig.2.1a) tend to operate at a constant speed on a straight-line trajectory, thus the model works under this assumption and doesn't consider any kind of longitudinal acceleration or centripetal acceleration due to curvature of the trajectory. On the vehicle's chassis act forces and torques as outlined in Fig.2.1b hence is possible to set up three equilibrium equations: a horizontal equilibrium equation, a vertical equilibrium equation and a rotational equilibrium equation as described in Eqs.2.1:

$$\begin{cases} F_{DP} = H_f + H_r \\ W = V_f + V_r \\ V_f \cdot (l_1 + l_2) - W \cdot l_2 + H_f \cdot (r_r - r_f) + M_f + M_r + F_{DP} \cdot (h - r_r) = 0 \end{cases} \tag{2.1}$$

Knowing that H_f, H_r are the horizontal forces at the wheel hub, V_f and V_r are the vertical forces at the wheel hub, M_f and M_r are the torques delivered by the engine, through the whole driveline to the wheels, F_{DP} is the drawbar pull that derives from the shear resistance encountered by the implements during the tilling operation and W is the total weight of the vehicle. Moreover, in addition to the three equilibrium equations is important to remember that the frame-side members impose a rigid body constraint keeping the distance between the front and rear axle

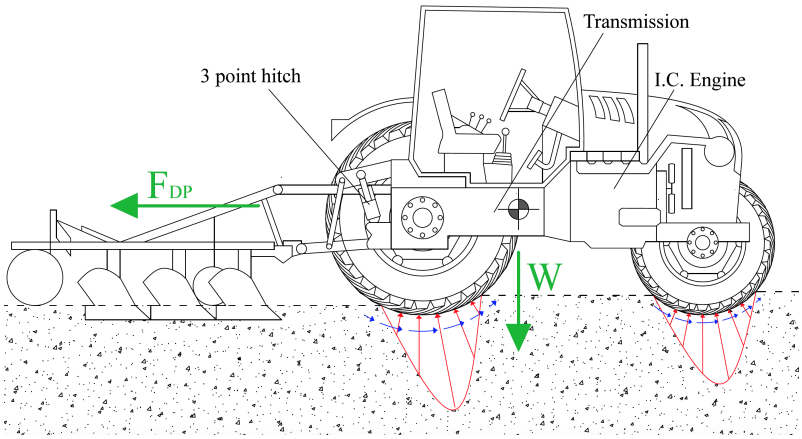

(a) Forces and stresses during tractor's operational conditions

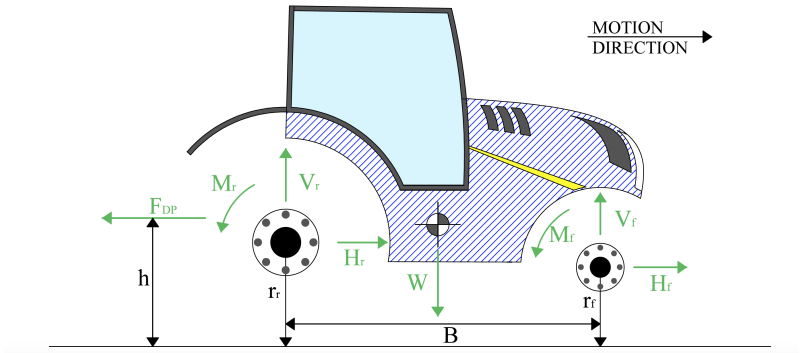

(b) Forces and torques acting on the tractor's chassis

constant, this fact means that the front and rear axle must have the same actual longitudinal speed as expressed below (Eq.2.2):

$$\omega_f \cdot r_f \cdot (1 - s_f) = \omega_r \cdot r_r \cdot (1 - s_r) \tag{2.2}$$

Knowing that ω_f and ω_r are the angular velocities of the front and rear wheels, and the slip of a generic wheel s_i is defined as in the following equation (Eq. 2.3):

$$s_i = \frac{\omega_i r_i - v}{\omega_i r_i} \tag{2.3}$$

Where the generic subscript "i" could be "f" or "r" depending on whether the axle is the front one or the rear one, moreover is also important to remark that r_f and r_r are the kinetic rolling radii of front and rear tires as defined by Kiss [22]. From Eq.2.3 clearly appears that s_i could be positive or negative, positive if the actual speed is smaller than the theoretical speed of the wheels (typically happening during pulling operations) and is called slip in the strictest sense of the word, negative if the actual speed is greater than the theoretical speed (typically happening during braking) and is defined as skid. As previously mentioned in the introduction, agricultural tractors typically present a mechanical front wheel drive transmission (M. F. W. D.) in which the power delivered by the internal combustion unit flows directly through the outer shaft of the transmission to the rear axle but using a pair of meshing gears to the front axle, without using any kind of central differential, exbhiting a closed differential behaviour. This type of constructive solution implies that is not possible to decouple the speed of front and rear wheels during steering

maneuver, to overcome this problem all the tractors have been produced having the front wheels with a theoretical tangential speed $2\% \div 7\%$ greater than rear wheels, the so called lead L of the front wheels. This kind of constructive architecture provides some advantages, in fact, the two meshing gears do not split the torque between the two axles in a fixed ratio but could freely variate depending on the requests arisen at the soil-tire interface, in addition to that is also a very efficient device; however presents the serious problem of torsional wind-up of the driveline, occurring at low-slippage level. As said before, the lead of the front wheels L is substantially a misalignment of the theoretical tangential speed that can be defined mathematically as in Eq.2.4:

$$L = \frac{\omega_f r_f - \omega_r r_r}{\omega_r r_r} \tag{2.4}$$

At this stage is important to introduce two mechanical quantities: K_W the front-to-rear ratio of kinetic rolling radii (Eq. 2.5) and τ_d the transmission front axle lead ratio (Eq. 2.6)

$$K_W = \frac{r_f}{r_r} \tag{2.5}$$

$$\tau_d = \frac{\omega_f}{\omega_r} \tag{2.6}$$

This allows to simplify the equation of L as below (Eq. 2.7):

$$L = \frac{\omega_f r_f - \omega_r r_r}{\omega_r r_r} = \frac{\omega_f r_f}{\omega_r r_r} - 1 = K_W \cdot \tau_d - 1 \tag{2.7}$$

The lead L depends on transmission front axle lead ratio τ_d, a quantity decided a priori by the manufacturer and on the front-to-rear ratio of kinetic rolling radii K_W, a quantity that is partially influenced by the operator through the regulation of the inflation pressure and partially by the manufacturer.

Moreover, by means of the definition expressed in Eq. 2.4, 2.5 and 2.6, the Eq.2.2 can be rephrased as:

$$s_r = (L + 1) \cdot s_f - L \tag{2.8}$$

Eq.2.8 highlights the fact that the slip of front and rear wheels are not independent but correlated through a linear equation in which the lead L plays a key role, in particular when the lead is positive there is a small region of the s_f-s_r plane in which the front axle tends to slip while the rear axle tends to skid, thus generating torsional wind-up[1] in the driveline, this problem occurs at low slippage level typically during on-highway motion and to be overcome generally the driver disengages the clutch of the M. F. W. D. mechanism, operating in a R. W. D. mode.

Considering the Eq.2.7 is possible to derive the governing equations of the tractor driveline

[1]Torsional wind-up is the phenomenon that happens when torque is applied and the rotation of one end of a shaft is greater than the one on the other end

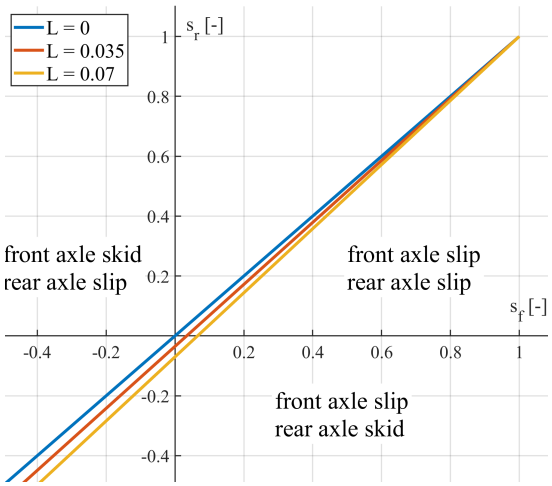

Figure 2.2: Linear relationship between the slip of the front and rear axle

$$\begin{cases} M_{tr} = M_r + \frac{L+1}{K_W} \cdot M_f \\ \omega_f = \frac{L+1}{K_W} \omega_r \\ M_e = \frac{M_{tr}}{\tau_{tr} \cdot \eta_{tr}} \\ \omega_e = \tau_{tr} \cdot \omega_r \end{cases} \tag{2.9}$$

Knowing that :

- M_{tr} is the torque at the transmission output shaft
- M_e is the torque delivered by the engine at the flywheel as a function of rotational speed and governor regulation
- η_{tr} transmission efficiency
- τ_{tr} gear ratio of the transmission

2.1.2 Equilibrium of the wheels and tire-soil interaction model

The soil is typically considered as a deformable medium in which the tires of the vehicle sink, the sinkage of the tire and therefore the contact patch between the soil and the wheel starts at an entry contact angle called θ_1 and ends at a rut recovery angle called θ_2, these two angles are not independent but related through the c_3 coefficient and was observed that the following relationship holds: $\theta_1 = c_3 \cdot \theta_2 = -0.125 \cdot \theta_2$. Furthermore, observing Fig. 2.4, is possible to understand that the soil and the wheel interact exchanging normal σ and shear τ stresses which are dependent on the contact angle θ and exhibit a peak at the angle θ_m. In order to keep the model as simple as possible we assumed that the right and left part of the tractor to behave in the same way, thus, remembering that b_f and b_r are the width of the contact areas, the resulting equations for the equilibrium of the front (Eqs. 2.10) and rear (Eqs. 2.11) wheels are reported below:

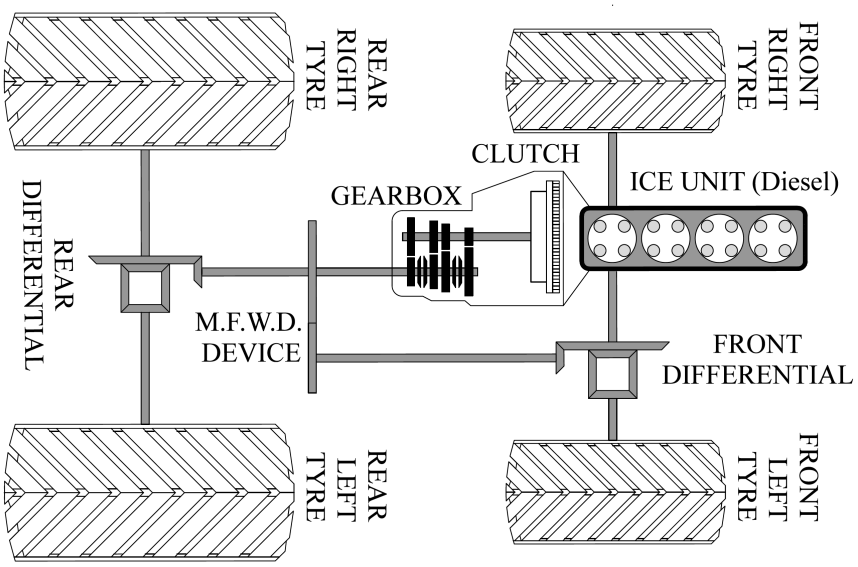

Figure 2.3: Simplified scheme of a MFWD driveline from a top view perspective

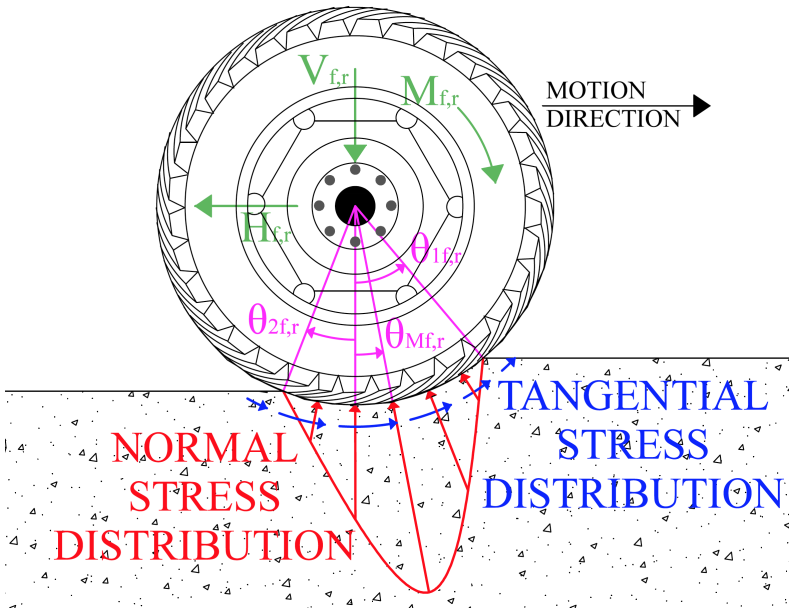

Figure 2.4: Forces, torques, normal and tangential stress distributions at the wheel-soil interface

$$\begin{cases} \frac{1}{2}H_f = b_f \cdot r_f \cdot \int_{\theta_{2,f}}^{\theta_{1,f}} (\tau_f \cdot cos\theta - \sigma_f \cdot sin\theta) d\theta \\ \frac{1}{2}V_f = b_f \cdot r_f \cdot \int_{\theta_{2,f}}^{\theta_{1,f}} (\tau_f \cdot sin\theta + \sigma_f \cdot cos\theta) d\theta \\ \frac{1}{2}M_f = b_f \cdot r_f^2 \cdot \int_{\theta_{2,f}}^{\theta_{1,f}} \tau_f d\theta \end{cases} \tag{2.10}$$

$$\begin{cases} \frac{1}{2}H_r = b_r \cdot r_r \cdot \int_{\theta_{2,r}}^{\theta_{1,r}} (\tau_r \cdot cos\theta - \sigma_r \cdot sin\theta) d\theta \\ \frac{1}{2}V_r = b_r \cdot r_r \cdot \int_{\theta_{2,r}}^{\theta_{1,r}} (\tau_r \cdot sin\theta + \sigma_r \cdot cos\theta) d\theta \\ \frac{1}{2}M_r = b_r \cdot r_r^2 \cdot \int_{\theta_{2,r}}^{\theta_{1,r}} \tau_r d\theta \end{cases} \tag{2.11}$$

The previous equilibrium equations (Eqs. 2.11, 2.10) derives from the vectorial composition of normal and shear stresses, the normal stresses on the front and rear wheels are stepwise defined as in Eqs. 2.12 and 2.13, while the shear stresses on the front and rear wheels are defined as in Eqs. 2.14 and 2.15.

Normal stresses are defined through the Bekker law [4, 5], later modified by Wong [42, 43], also known as pressure-sinkage relationship (Eqs. 2.12 2.13), in which holds the assumption that the behavior of the wheel is comparable to a rectangular plate sinking into the soil due to a vertical pressure distribution.

$$\sigma_f(\theta) = \begin{cases} (\frac{k_{c,f}}{b_f} + k_{\phi,f}) \cdot r_f^n \cdot [cos(\theta_{1,f} - \frac{\theta - \theta_{2,f}}{\theta_{m,f} - \theta_{2,f}}) - cos(\theta_{1,f})]^n; \theta_{2,f} \leq \theta \leq \theta_{m,f} \\ (\frac{k_{c,f}}{b_f} + k_{\phi,f}) \cdot r_f^n \cdot [cos(\theta) - cos(\theta_{1,f})]^n; \theta_{m,f} \leq \theta \leq \theta_{1,f} \end{cases} \tag{2.12}$$

$$\sigma_r(\theta) = \begin{cases} (\frac{k_{c,r}}{b_r} + k_{\phi,r}) \cdot r_r^n \cdot [cos(\theta_{1,r} - \frac{\theta - \theta_{2,r}}{\theta_{m,r} - \theta_{2,r}}) - cos(\theta_{1,r})]^n; \theta_{2,r} \leq \theta \leq \theta_{m,r} \\ (\frac{k_{c,r}}{b_r} + k_{\phi,r}) \cdot r_r^n \cdot [cos(\theta) - cos(\theta_{1,r})]^n; \theta_{m,r} \leq \theta \leq \theta_{1,r} \end{cases} \tag{2.13}$$

Where:

- r_f, r_r is the kinetic rolling radius of front and rear wheels
- b_f, b_r is the width of front and rear wheels
- $k_{c,f}$, $k_{c,r}$ is the soil cohesion related parameter of front and rear wheels
- $k_{\phi,f}$, $k_{\phi,r}$ is the internal friction angle related parameter of front and rear wheels
- n is the Bekker sinkage exponent
- $\theta_{1,f}$ $\theta_{1,r}$ entry angle of front and rear wheels
- $\theta_{m,f}$ $\theta_{m,r}$ contact angle at which the normal stresses peaks, defined by means of Eqs. 2.18, 2.19
- $\theta_{2,f}$ $\theta_{2,r}$ rut recovery angle defined by means of Eqs. 2.20, 2.21

The shear stresses acting beneath the wheels are defined following the non-linear approach proposed by Janosi-Hanamoto [19] (Eqs. 2.14, 2.15), which defined a modified version of the Mohr-Coulomb failure envelope:

$$\tau_f(\theta) = [c_f + \sigma_f(\theta) \cdot tan(\phi)] \cdot (1 - e^{-\frac{j_f}{j_{0,f}}}) \tag{2.14}$$

$$\tau_r(\theta) = [c_r + \sigma_r(\theta) \cdot tan(\phi)] \cdot (1 - e^{-\frac{j_r}{j_{0,r}}}) \tag{2.15}$$

Where:

- c_f, c_r is the soil coehesion related to front and rear wheels
- ϕ is the internal friction angle of the soil
- j_f, j_r is the shear displacement of the soil related to the front and rear wheels and could be computed by means of Eqs. 2.16, 2.17
- $j_{0,f}$, $j_{0,r}$ is the shearing deformation modulus that could be described as the shear displacement when the shear stress peaks

$$j_f = r_f \cdot [\theta_{1,f} - \theta - (1 - s_f) \cdot (sin(\theta_{1,f}) - sin(\theta))] \tag{2.16}$$

$$j_f = r_r \cdot [\theta_{1,r} - \theta - (1 - s_r) \cdot (sin(\theta_{1,r}) - sin(\theta))] \tag{2.17}$$

$$\theta_{m,f} = (c_1 + c_2 \cdot |s_f|) \cdot \theta_{1,f} \tag{2.18}$$

$$\theta_{m,r} = (c_1 + c_2 \cdot |s_r|) \cdot \theta_{1,r} \tag{2.19}$$

$$\theta_{2,f} = c_3 \cdot \theta_{1,f} \tag{2.20}$$

$$\theta_{2,r} = c_3 \cdot \theta_{1,r} \tag{2.21}$$

2.1.3 The derivation of the power delivery efficiency

The power delivery efficiency η_T is described as the goodness of the process in transferring engine power into useful work, is typically defined as the ratio between the drawbar power and the power delivered by the internal combustion engine (Eq.2.22)

$$\eta_T = \frac{F_{DP} \cdot v}{M_e \cdot \omega_e} \tag{2.22}$$

Furthermore, through a series of mathematical passages, readable below, is possible to obtain the expression of η_T as the product of three efficiency terms (Eq.2.23):

- η_{tr} the Transmission Efficiency
- η_S the Slip Efficiency

- η_M the Motion Efficiency

$$\eta_T = \eta_{tr} \cdot \eta_S \cdot \eta_M \tag{2.23}$$

As a consequence of the rigid body constraint acting on the vehicle, the actual speed of the front and rear wheels must be equal to the real speed of the vehicle, thus the following relationship (Eq.2.24) holds:

$$v = \omega_f \cdot r_f \cdot (1 - s_f) = \omega_r \cdot r_r \cdot (1 - s_r) \tag{2.24}$$

Subsequently, substituting the expression of the real speed of the vehicle (v) and knowing that the drawbar pull F_{DP} is composed by the summation of horizontal thrust of the front (H_f) and rear (H_r) wheels, is possible to rewrite Eq.2.22 as in Eq.2.25:

$$\eta_T = \frac{(H_f + H_r)v}{M_e\omega_e} = \frac{H_f\omega_f r_f(1 - s_f) + H_r\omega_r r_r(1 - s_r)}{M_e\omega_e} \tag{2.25}$$

$$\eta_T = \frac{H_f\omega_f r_f + H_r\omega_r r_r}{H_f\omega_f r_f + H_r\omega_r r_r} \cdot \frac{H_f\omega_f r_f(1 - s_f) + H_r\omega_r r_r(1 - s_r)}{M_e\omega_e} =$$

$$= \frac{H_f\omega_f r_f + H_r\omega_r r_r}{M_e\omega_e} \cdot \frac{H_f\omega_f r_f + H_r\omega_r r_r - H_f\omega_f r_f s_f - H_r\omega_r r_r s_r}{H_f\omega_f r_f + H_r\omega_r r_r} =$$

$$= \frac{H_f\omega_f r_f + H_r\omega_r r_r}{M_e\omega_e} \cdot (1 - \frac{H_f\omega_f r_f s_f + H_r\omega_r r_r s_r}{H_f\omega_f r_f + H_r\omega_r r_r}). \tag{2.26}$$

Subsequently isolating the term $\omega_f r_f$ in Eq. 2.24 and inserting it in Eq. 2.26:

$$\omega_f r_f(1 - s_f) = \omega_r r_r(1 - s_r) \rightarrow \omega_f r_f = \frac{\omega_r r_r(1 - s_r)}{(1 - s_f)}$$

$$\eta_T = \frac{H_f\omega_f r_f + H_r\omega_r r_r}{M_e\omega_e} \cdot (1 - \frac{H_f\frac{1-s_r}{1-s_f}\omega_r r_r s_f + H_r\omega_r r_r s_r}{H_f\frac{1-s_r}{1-s_f}\omega_r r_r + H_r\omega_r r_r}).$$

$$= \frac{H_f\omega_f r_f + H_r\omega_r r_r}{M_e\omega_e} \cdot (1 - \frac{(1 - s_r)H_f s_f + (1 - s_f)H_r s_r}{(1 - s_r)H_f + (1 - s_f)H_r}).$$

The definition of pull distribution factor is reported below in Eq. 2.27

$$K_P = \frac{H_r}{H_f + H_r} = \frac{H_r}{F_{DP}} \tag{2.27}$$

Then is possible to get the expression of H_f and H_r depending on K_P and F_{DP}:

$$H_f = F_{DP} \cdot (1 - K_P)$$

$$H_r = F_{DP} \cdot K_P$$

$$\eta_T = \frac{H_f\omega_f r_f + H_r\omega_r r_r}{M_e\omega_e} \cdot (1 - \frac{(1 - s_r)s_f F_{DP}(1 - K_P) + (1 - s_f)s_r F_{DP}K_P}{(1 - s_r)F_{DP}(1 - K_P) + (1 - s_f)s_r F_{DP}K_P}) =$$

$$= \frac{H_f\omega_f r_f + H_r\omega_r r_r}{M_e\omega_e} \cdot (1 - \frac{(1-s_r)s_f(1-K_P) + (1-s_f)s_r K_P}{(1-s_r)(1-K_P) + (1-s_f)K_P}) =$$

$$= \frac{H_f\omega_f r_f + H_r\omega_r r_r}{M_e\omega_e} \cdot (1 - \frac{(1-s_r)s_f - (s_f - s_r)K_P}{(1-s_r) - (s_f - s_r)K_P}). \tag{2.28}$$

The term between the two round brackets is defined as slip efficiency η_S:

$$\eta_S = 1 - \frac{(1-s_r)s_f - (s_f - s_r)K_P}{(1-s_r) - (s_f - s_r)K_P}. \tag{2.29}$$

Now introducing the front-to-rear ratio of kinetic rolling radii $K_W = \frac{r_f}{r_r}$ and the the transmission front axle lead ratio τ_d the following relationship holds:

$$\frac{\omega_f r_f - \omega_r r_r}{\omega_r r_r} = K_W \cdot \tau_d - 1 \tag{2.30}$$

From this equation is possible to get:

$$\omega_f r_f = K_W \cdot \tau_D \cdot \frac{\omega_e}{\tau_{tr}} \cdot r_r$$

$$\omega_r r_r = \frac{\omega_e}{\tau_{tr}} \cdot r_r$$

Leading to

$$\eta_T = H_f \cdot K_W \cdot \frac{\tau_D}{\tau_{tr}} \cdot r_r + H_r \cdot \frac{r_r}{\tau_{tr}} \cdot M_e$$

The torque provided by the engine can be computed in the following manner:

$$M_e = \frac{M_r + \tau_d \cdot M_f}{\tau_{tr} \cdot \eta_{tr}}$$

$$\eta_T = \frac{H_f \cdot K_W \cdot \tau_D \cdot r_r + H_r \cdot r_r}{M_r + \tau_D \cdot M_f} \cdot \eta_{tr} \cdot \eta_S = \frac{H_f \cdot K_W \cdot \tau_D + H_r}{\frac{\tau_d}{r_r} \cdot M_f + \frac{M_r}{r_r}} \cdot \eta_{tr} \cdot \eta_S$$

$$K_W \cdot \tau_d = L + 1$$

$$\frac{\tau_d}{r_r} = \frac{L+1}{r_f}$$

$$\eta_T = \frac{H_f \cdot (L+1) + H_r}{\frac{M_f}{r_f} \cdot (L+1) + \frac{M_r}{r_r}} \cdot \eta_{tr} \cdot \eta_S$$

The first term is defined as the motion efficiency of the vehicle

$$\eta_M = \frac{H_f \cdot (L+1) + H_r}{\frac{M_f}{r_f} \cdot (L+1) + \frac{M_r}{r_r}}$$

Finally

$$\eta_T = \eta_{tr} \cdot \eta_S \cdot \eta_M$$

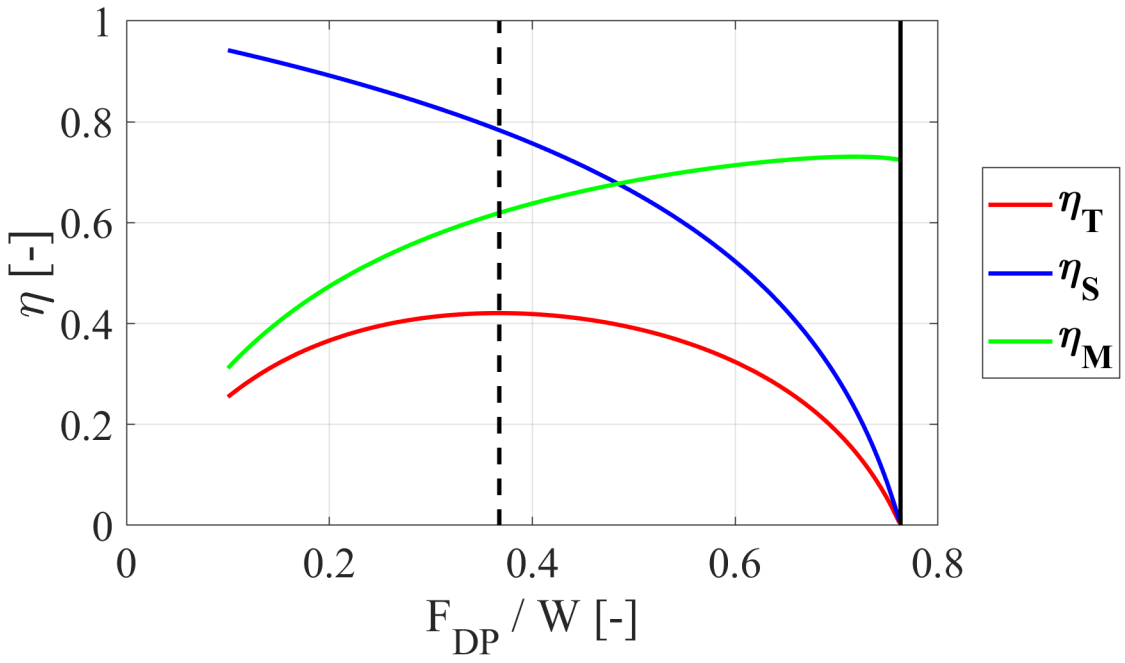

Figure 2.5: Efficiencies plot concerning a medium row crop agricultural tractor running on a deformable soil

2.1.4 The solution algorithm procedure

For a tractor, with given constructive features, running on a deformable soil with specific mechanical properties and with an imposed value of drawbar pull (F_{DP}), through Eq.2.10 and Eq.2.11 inserted in the global system of equilibrium equations (Eqs.2.1) and accounting for the rigid body constraint (Eq.2.8) is possible to built up the following mixed system of integral and linear equations Eqs.2.31:

$$\begin{cases} F_{DP} = 2b_f r_f \int_{\theta_{2,f}}^{\theta_{1,f}} (\tau_f cos\theta - \sigma_f sin\theta) d\theta + 2b_r r_r \int_{\theta_{2,r}}^{\theta_{1,r}} (\tau_r cos\theta - \sigma_r \sin\theta) d\theta \\ W = 2b_f r_f \int_{\theta_{2,f}}^{\theta_{1,f}} (\tau_f sin\theta + \sigma_f cos\theta) d\theta + 2b_r r_r \int_{\theta_{2,r}}^{\theta_{1,r}} (\tau_r sin\theta + \sigma_r cos\theta) d\theta \\ 2b_f r_f (l_1 + l_2) \int_{\theta_{2,f}}^{\theta_{1,f}} (\tau_f sin\theta + \sigma_f cos\theta) d\theta + 2b_f r_f (r_r - r_f) \int_{\theta_{2,f}}^{\theta_{1,f}} (\tau_f cos\theta + \sigma_f sin\theta) d\theta + ... \\ ... + 2b_f r_f^2 \int_{\theta_{2,f}}^{\theta_{1,f}} \tau_f d\theta + 2b_r r_r^2 \int_{\theta_{2,r}}^{\theta_{1,r}} \tau_r d\theta - W l_2 + F_{DP}(h - r_r) = 0 \\ s_r = (L+1) s_f - L \end{cases} \tag{2.31}$$

The system 2.31 is composed by four equations and depends on four main unknowns:

- s_f slip of the front wheels
- s_r slip of the rear wheels
- $\theta_{1,f}$ front wheels entry angle

- $\theta_{1,r}$ rear wheels entry angle

The previously outlined system of equations (Eqs.2.31) was solved through the Trust Region Dogleg Algorithm implemented in MATLAB (Mathworks, Inc., MA, USA) and the evaluation of the integrals using the Simpson's method.

Once s_f, s_r, $\theta_{1,f}$ and $\theta_{1,r}$ have been computed, by means of a back-substitution in Eq.2.10 and in Eq.2.11 is possible to get the numerical value of forces and torques acting on the front and rear hub (H_f, V_f, M_f, H_r, V_r, M_r).
The computation of the torque at each single wheel hub allows to determine the Torque Distibution Factor $K_T = \frac{M_r}{M_r+M_f}$ which is not defined a-priori and is typically unknown by the tractor's manufacturer, for this reason is of particular interest.

2.2 Gradient based method for the analysis of the influence of the tractor design parameters on the power delivery efficiency

The previously described mathematical model was used to run a complete set of 32768 simulations, each simulation corresponds to a specific tractor configuration working on LETE sand, the aim was to verify which are the most influential constructive parameters on the power delivery efficiency. Before launching the complete set of 32768 simulations we perform preliminary simulations to assess which is the value of drawbar pull F_{DP} (see the black dashed line in Fig.2.5) that maximize the power delivery efficiency of a generic row-crop tractor in a standard configuration, once found this value was kept constant during the simulations.

Symbol	Value	Unit of measure
c_1	0.200	$[-]$
c_2	0.300	$[-]$
c_3	-0.125	$[-]$
c_f	0.900	$[kPa]$
c_r	0.900	$[kPa]$
$j_{0,f}$	$11.5 \cdot 10^{-3}$	$[m]$
$j_{0,r}$	$11.5 \cdot 10^{-3}$	$[m]$
$k_{c,f}$	$1.560 \cdot 10^5$	$[Nm^{-n-1}]$
$k_{c,r}$	$1.560 \cdot 10^5$	$[Nm^{-n-1}]$
$k_{\phi,f}$	$4.530 \cdot 10^6$	$[Nm^{-n-2}]$
$k_{\phi,r}$	$4.530 \cdot 10^6$	$[Nm^{-n-2}]$
n	0.806	$[-]$
ϕ	0.550	$[rad]$

Table 2.1: LETE sand soil parameters

Five tractor design parameters were varied on eight steps with respect to the tractor standard configuration (Table 2.2), thus creating a regular grid, for a total of $8^5 = 32768$ simulations. The tractor design parameters used for the parametric analysis are listed below:

- $K_M = \frac{l_1}{B}$ the static mass distribution

Symbol	Value	Unit of measure
W	87.2	$[-]$
r_r	0.900	$[m]$
b_r	0.750	$[m]$
b_f	0.600	$[m]$
η_{tr}	0.867	$[-]$
K_M	0.580	$[-]$
B	2.88	$[m]$
K_W	0.78	$[-]$
L	$6.590 \cdot 10^{-2}$	$[-]$
h	$0.560 \cdot 10^{6}$	$[m]$

Table 2.2: Row crop tractor parameters in the standard configuration

- B wheelbase
- K_W the front to rear ratio of kinetic rolling radii
- L the lead of the front wheels
- h the drawbar height

The range of variation of the previously listed parameters and those that have been kept constant are reported in the following Table 2.3:

Symbol	Value	Unit of measure
W	87.2	$[-]$
r_r	0.900	$[m]$
b_r	0.750	$[m]$
b_f	0.600	$[m]$
η_{tr}	0.867	$[-]$
F_{DP}	27.5	$[kN]$
K_M	$[0.3 - 0.8]$	$[-]$
B	$[2.5 - 3.5]$	$[m]$
K_W	$[0.7 - 1.0]$	$[-]$
L	$[0.0 - 0.07]$	$[-]$
h	$[0.3 - 0.7]$	$[m]$

Table 2.3: Tractor parameters used in the parametric analysis

The definition domain over which the simulations have been performed is symbolically defined below in Eq. 2.32:

$$\Omega = K_M \times B \times K_W \times L \times h \tag{2.32}$$

For each simulation, the power delivery efficiency η_T, the slip efficiency η_S and the motion efficiency η_M have been computed and assumed as the main parameters for the performance evaluation of the tractor in a certain configuration. In order to investigate if a certain variable influences the efficiencies of the vehicle a gradient method, based on the central difference scheme, was implemented. The theoretical

background on which relies the gradient method is that, given a multivariable function $f(x_1, x_2, ..., x_n)$ the gradient ∇f is a vector identified by the directional cosines and is perpendicular to the level curve, moreover the gradient highlights the direction of maximum slope of the function. Is important to remark that if in the point $\overline{X_0} = (x_{1,0}; x_{2,0}; ...; x_{n,0})$ the direction cosine of $(\nabla f(\overline{X_0}))$ along a given coordinate is null, then $\nabla f(\overline{X_0})$ is orthogonal to this direction and that coordinate does not play any influencing role on the function f in this specific point. In this study the efficiencies η_T, η_M and η_S have assumed as functions of five constructive parameters:

$$\hat{\eta_S} = \hat{\eta_S}(K_M^*, B*, K_W^*, L^*, h^*) \tag{2.33}$$

$$\hat{\eta_M} = \hat{\eta_M}(K_M^*, B*, K_W^*, L^*, h^*) \tag{2.34}$$

$$\hat{\eta_T} = \hat{\eta_T}(K_M^*, B*, K_W^*, L^*, h^*) \tag{2.35}$$

The fact that the efficiencies reported in Eqs.2.33, 2.34, 2.35 have been labeled with the circumflex accent means that they have been computed at a constant value of drawbar pull F_{DP}: this value of drawbar pull is the one which maximizes the power delivery efficiency of a medium row crop agricultural tractor and the value is the one indicated by the black dashed line in Fig. 2.5. Furthermore, all the constructive parameters labeled with the symbol * means that these are scaled variables, in particular:

- $K_M^* = \frac{K_M - K_M^{med}}{\frac{1}{2}\cdot(K_M^{max} - K_M^{min})}$ is the scaled static mass distribution
- $B^* = \frac{B - B^{med}}{\frac{1}{2}\cdot(B^{max} - B^{min})}$ is the scaled wheelbase
- $K_W^* = \frac{K_W - K_W^{med}}{\frac{1}{2}\cdot(K_W^{max} - K_W^{min})}$ is the scaled front to rear ratio of kinetic rolling radii
- $L^* = \frac{L - L^{med}}{\frac{1}{2}\cdot(L^{max} - L^{min})}$ is the scaled lead of the front wheels
- $h^* = \frac{h - h^{med}}{\frac{1}{2}\cdot(h^{max} - h^{min})}$ is the scaled drawbar height

The previously described scaling operation allows us a direct comparison among the variables and in this way the definition domain was reduced to a 5D bi-unitary domain:

$$\Omega^* = [-1; 1] \times [-1; 1] \times [-1; 1] \times [-1; 1] \times [-1; 1] \tag{2.36}$$

After the scaling operation was necessary to compute the gradients inside the multidimensional domain Ω^*, all the partial derivative have been calculated thanks to the central difference scheme and then the direction cosines of the five variables have been represented in a bar plot with the aim to understand the degree of influence on the different efficiencies of the tractor; the least significant parameters have been neglected from the regression surface analysis, described in the following section.

2.3 Simplified regression surfaces based on simulations results

To simplify the results coming from the simulations concerning different tractor configurations and to understand which parameters played a primary role in the tractor power delivery efficiency, it was decided to perform a fitting with a polynomial regression surface. In order to keep the polynomial regression model as simple as possible was decided to use the lowest polynomial function that allows to describe the observed trends, furthermore we de also accounted just the for significant variables emerged from the gradient analysis; the least square methods were used for the determination of the regression coefficients, indeed the goodness of the fit was provided thanks to the coefficient of determination R^2.

2.4 Experimental model validation

The mathematical model proposed in the previously outlined sections presents a high level of complexity, involving many physical/empirical parameters and linear/non-linear equations; in order to assess the fairness and accuracy of the model a validation carried out through a comparison with experimental tests is required. Experimental tests mean drawbar tests in which the testing tractor, coupled through a tow bar (chain) and a load cell to measure the drawbar force, pulls a braking tractor; adjusting the throttle position and the engaged gears of the braking tractor it is possible to regulate the drawbar force applied and the motion speed. Drawbar tests were initially carried out in open field conditions with different tractors and with different mass distributions. From a practical point of view, the experiment consists of several trials performed at different values of drawbar pull, the aim was to explore the largest possible portion of the definition domain of the power delivery efficiency curve. Once the tests were completed, a comparison was made between measured data and simulated data from the model, the soil parameters were obtained using the ordinary least squares method contextualized in a reverse engineering process, the goodness of the fitting is computed using the coefficient of determination R^2.

2.4.1 Drawbar tests in open-field conditions

Drawbar tests on different soil conditions

The tests have been performed using a Case IH Maxxum 115 (CNH Industrial SpA, Italy), equipped with a set of brand new radial tire (Continental AC65, Continental AG, Hannover, Germany), the features of the vehicle are reported in the table below. On the testing tractor a CAN-Bus based acquisition system (CanCase XL Log, Vector Informatik, GmbH, Stuttgart, Germany) have been installed that allows measuring the engine rotational speed, the engine torque and other vehicle-related parameters; a GPS receiver (IPESpeed, IPETronik GmbH, Baden Baden, Germany) records the actual speed of the vehicle, a phonic wheel measures the theoretical speed, torsiometers installed on the hubs measure forces and torques hence all the characteristics efficiencies can be obtained.

Physical quantity	Value	Unit of measure
Engine nominal power	85	$[kW]$
Static mass	7380	$[kg]$
front axle static mass	44	[%]
Rear tires	$600/65R38$ - 1bar	$[mult]$
Front tires	$480/65R28$ - 1bar	$[mult]$
Rolling radius of rear tires (BSI 2017)	0.833	[m]
Transmission	SPS - 16 Forward - 16 Rearward	[/]
Front axle lead	1.26	[%]

Table 2.4: Tractor parameters used in the open field validation concerning a Case IH Maxxum 115

Figure 2.6: Drawbar tests in open-field conditions, is clearly visible the front pulling tractor (Case IH Maxxum 115) and the rear braking tractor (New Holland T7-260)

Drawbar tests with different mass distributions

To understand if the model was reliable even when the vehicle is operating in different configurations, various experiments were carried out with a New Holland T7-260 tractor in which the overall weight was kept constant but the mass distribution was changed. The variations in mass distribution were obtained through a hydraulically operated device that allowed to approach and remove the ballast towards the front of the tractor, with particular reference to the tests carried out in this experimental campaign, three different mass distributions were tested: one with the device fully extended, one with the device completely closed and one with the ballast mounted on the three-point hitch of the pulling tractor. All the characteristics of the pulling tractors are reported in Table 2.4.

Since the pulling tractor was quite heavy and was able to exert high traction force it was necessary to equip the braking tractor with a plough carried on the rear three-point hitch, as is possible to see in Fig.2.9; the aim to be pursued was to increase the weight and therefore the braking potential of the rear tractor:

Figure 2.7: Detail of the load cell used for drawbar force measurements

(a) Detail of the device for the position control of the front ballast - CLOSED position

(b) Detail of the device for the position control of the front ballast - OPEN position

Physical quantity	Value	Unit of measure
Engine nominal power	194	$[kW]$
Engine nominal torque	1349	$[Nm]$
Static mass [ballasted]	9590	$[kg]$
front axle static mass [ballasted]	$[56.31 - 58.76 - 32.46]$	$[\%]$
Rear tires	$710/70R38$ - 1.2bar	$[mult]$
Front tires	$600/65R28$ - 1.2bar	$[mult]$
Wheelbase	2.888	$[m]$
Rolling radius of rear tires (BSI 2017)	0.925	$[m]$
Transmission	FPS - 16 Forward - 8 Rearward	$[mult]$
Front axle lead	6.5	$[\%]$

Table 2.5: Tractor parameters used in the open field validation concerning a New Holland T7-260

Figure 2.9: Rear view of pulling/braking tractors ensemble, is clearly visible the rear mounted plough

Chapter 3

Results and Discussion

Organizational remarks

The Results and Discussion chapter is organized as follows:

- A first section called **Model Validation** in which is shown, through experimental data, that the proposed model is reliable and capable of reproducing the traction performance of a tractor operating under different conditions, both in terms of mass distribution and soil textures.

- A second section called **Torque Distribution Factor** K_T which clarifies how the torque produced by the engine is distributed between the two axles in a M.F.W.D. agricultural tractor.

- A third section called **Gradient Method** where, through the study of the gradient of the power delivery efficiency η_T, the expression for determining the optimal mass distribution was determined.

3.1 Model Validation

The model proposed was validated using experimental data coming from drawbar tests, different layout of the tractor and different soil textures have been investigated. The analysis of the obtained data was then carried out through three different graphs:

- A first graph (a) in which there is a comparison between the experimental and simulated power delivery efficiency curves (η_T) as a function of the drawbar force divided by the vehicle weight (F_{DP}/W).

- A second graph (b) showing the simulated and measured power delivery efficiency, the more the dispersion of points is distributed as a straight line inclined by 45 degrees, the more accurate is the model.

- A third graph (c) showing a scatter plot of the residuals, if the points appear to be dispersed uniformly and randomly then the model is free of systematic errors.

3.1.1 Drawbar tests in open field conditions

Drawbar tests on different soil conditions

Parameters	Tilled Clayey Loam	Tilled Loam	Untilled Loam
c_1 $[-]$	0.4840	0.4546	0.4235
c_2 $[-]$	0.4665	0.2900	0.2588
n $[-]$	1.1815	1.1600	1.1632
k_c $[Nm^{-n-1}]$	$1.2981 \cdot 10^6$	$7.6195 \cdot 10^5$	$1.7267 \cdot 10^6$
k_ϕ $[Nm^{-n-2}]$	$5.1746 \cdot 10^6$	$1.8379 \cdot 10^6$	$5.2433 \cdot 10^6$
c $[Pa]$	$4.7231 \cdot 10^4$	$4.0580 \cdot 10^4$	$3.4818 \cdot 10^4$
ϕ $[rad]$	0.8047	0.7328	0.7712
j_0 $[m]$	0.0950	0.0886	0.0789
η_{tr} $[-]$	0.8600	0.8668	0.8742

Table 3.1: Mechanical properties of different soils and transmission efficiency η_{tr}

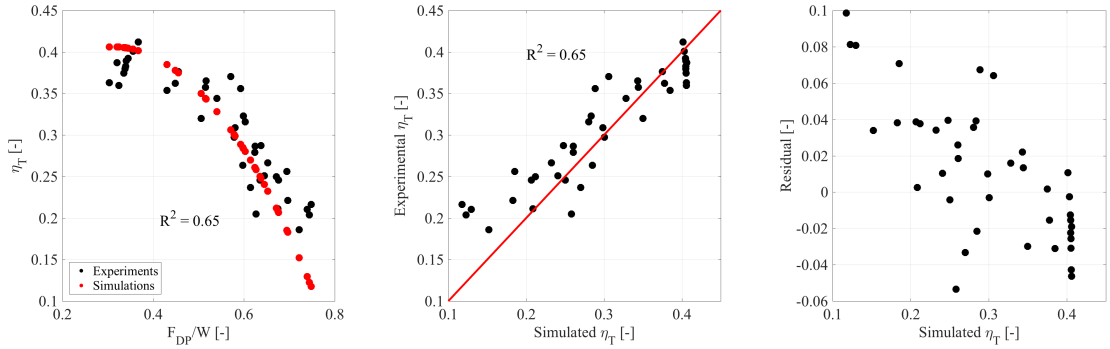

(a) Simulations vs Experiments in the $\frac{F_{DP}}{W}$ - η_T space

(b) Comparison of simulated η_T and experimental η_T

(c) Scatter plot of the residual

Figure 3.1: Model validation concerning a MFWD row-crop tractor running on a **tilled clayey loam** soil

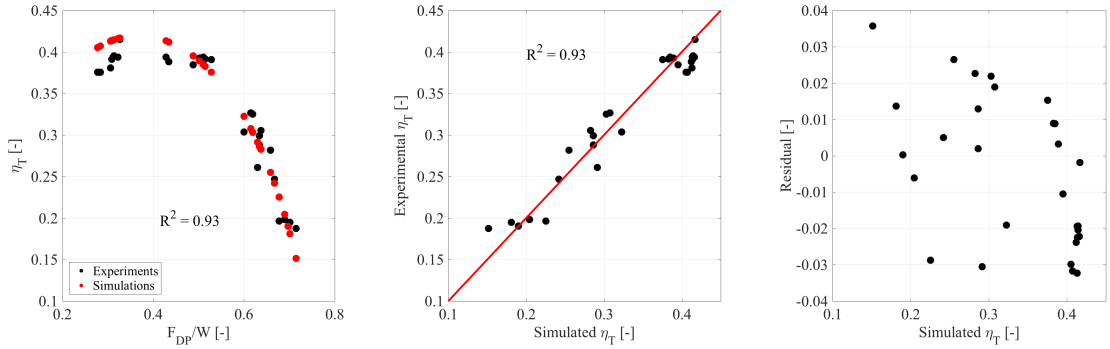

(a) Simulations vs Experiments in the $\frac{F_{DP}}{W}$ - η_T space

(b) Comparison of simulated η_T and experimental η_T

(c) Scatter plot of the residual

Figure 3.2: Model validation concerning a MFWD row-crop tractor running on a **tilled loam** soil

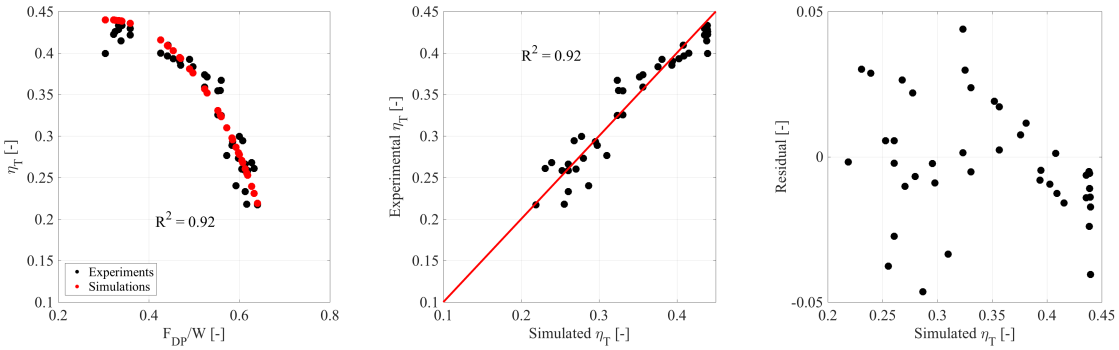

(a) Simulations vs Experiments in the $\frac{F_{DP}}{W}$ - η_T space

(b) Comparison of simulated η_T and experimental η_T

(c) Scatter plot of the residual

Figure 3.3: Model validation concerning a MFWD row-crop tractor running on an **untilled loam** soil

	Tilled Clayey Loam	Tilled Loam	Untilled Loam
R^2	0.65	0.93	0.92

Table 3.2: Fitting accuracy of the model on different soils

Comparing simulations and experimental data on three different soil conditions appears a satisfactory correspondence both in terms of fitting and of residuals, on **tilled loam** and on **untilled loam** the results are very accurate $R^2 > 0.92$, indeed on a **tilled clayey loam** terrain the coefficient is a bit lower $R^2 = 0.65$ probably due to slightly more dispersed measured values.

Drawbar tests with different mass distributions

Parameters	Numerical values
c_1 $[-]$	0.4176
c_2 $[-]$	0.2077
n $[-]$	1.1760
k_c $[Nm^{-n-1}]$	$1.2072 \cdot 10^6$
k_ϕ $[Nm^{-n-2}]$	$2.5987 \cdot 10^6$
c $[Pa]$	$2.7919 \cdot 10^4$
ϕ $[rad]$	0.7518
j_0 $[m]$	0.0628
η_{tr} $[-]$	0.8843

Table 3.3: Values concerning the soil properties and the transmission efficiency η_{tr} for the validation performed with different tractor's mass distributions

	Front Closed Ballast	Front Open Ballast	Rear Ballast
R^2	0.41	0.64	0.78

Table 3.4: Fitting accuracy of the model concerning a tractor with different mass distribution

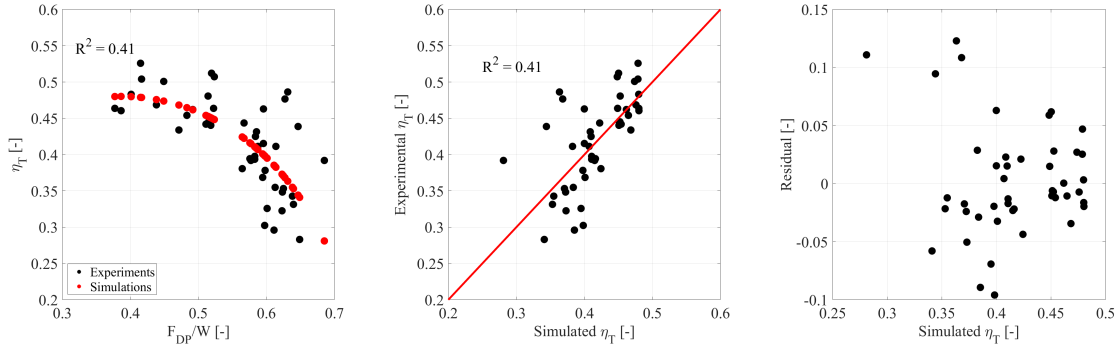

(a) Simulations vs Experiments in the $\frac{F_{DP}}{W}$ - η_T space (b) Comparison of simulated η_T and experimental η_T (c) Scatter plot of the residual

Figure 3.4: Model validation concerning a MFWD row-crop tractor with the 56.31% of the mass acting on the front axle while is running on a light-tilled loam soil

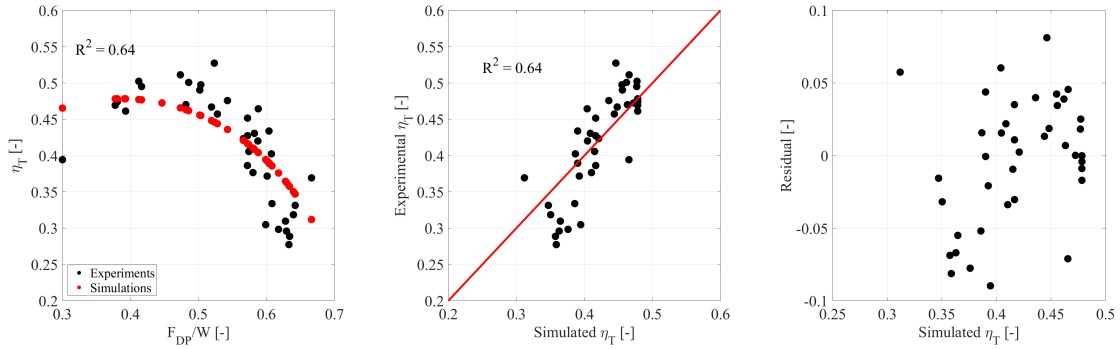

(a) Simulations vs Experiments in the $\frac{F_{DP}}{W}$ - η_T space (b) Comparison of simulated η_T and experimental η_T (c) Scatter plot of the residual

Figure 3.5: Model validation concerning a MFWD row-crop tractor with the 58.76% of the mass acting on the front axle while is running on a light-tilled loam soil

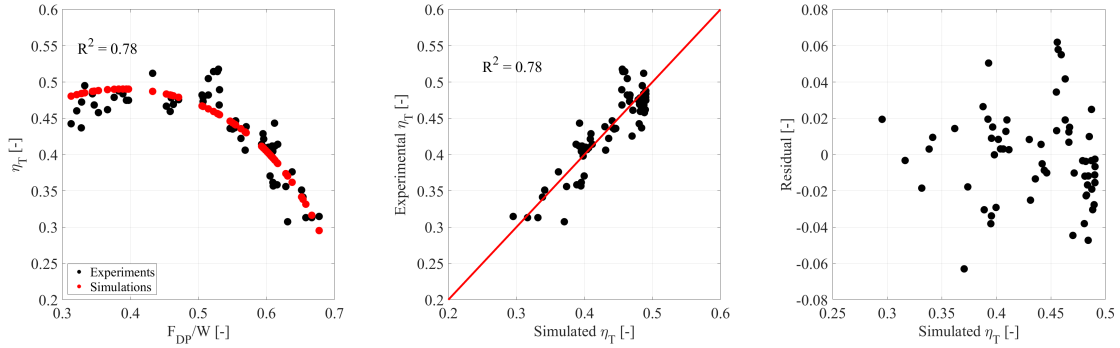

(a) Simulations vs Experiments in the $\frac{F_{DP}}{W}$ - η_T space (b) Comparison of simulated η_T and experimental η_T (c) Scatter plot of the residual

Figure 3.6: Model validation concerning a MFWD row-crop tractor with the 32.46% of the mass acting on the front axle while is running on a light-tilled loam soil

From the comparison of experimental and simulated data is clearly visible that even for different mass distributions the model is able to provide rather reliable

results, however, they are in terms of R^2 slightly worse than the tests on different types of terrain; it was hypothesized that this was due to the fact that tests were carried out on a high extension field that during the day exhibits humidity variations but in the fitting process it was assumed that the properties of the soil were constant. In addition to that, slightly more scattered measurements were found, especially in tests with the front ballast, thus inevitably degrading the quality of the fitting. Nevertheless, we believe that even in this case the results are satisfactory and able to depict the real behavior of the vehicle in terms of tractive performances. A careful analysis of the graphs (a), (b) and (c) of Fig.3.4, Fig.3.5 and Fig.3.6 shows that the clouds of experimental points are strictly distributed around the curve deriving from the simulations, that the points (η_T^{sim}, η_T^{exp}) are dispersed according to a straight line inclined at 45 degrees and that the residual plots are randomly spaced in the domain, underlining the lack of systematic errors.

3.2 Torque Distribution Factor K_T

The comparison of experimental and simulated data, previously shown, allows to state that the model proposed is reliable and therefore able to describe the behavior of a tractor under operational conditions. Nevertheless, as mentioned in the Materials and Methods chapter, the Torque Distribution Factor K_T[1] is not a value defined a priori by the manufacturer and many meetings with agricultural vehicle manufacturers revealed that the torque distribution factor in M.F.W.D. vehicles was an aspect that has not yet been fully clarified, hence a clarification on this aspect seemed to be necessary.
The results shown below (Fig.3.7) are the output of numerical simulations, the two reference vehicles are the same as those used in the validation phase: a Case-IH Maxxum-115 and a New Holland T7-260, running on a Tilled Loam soil, the mechanical properties of the soil are reported in Tab.3.1 and the constructive features of the tractors are reported in Tab.2.4 and Tab.2.5.

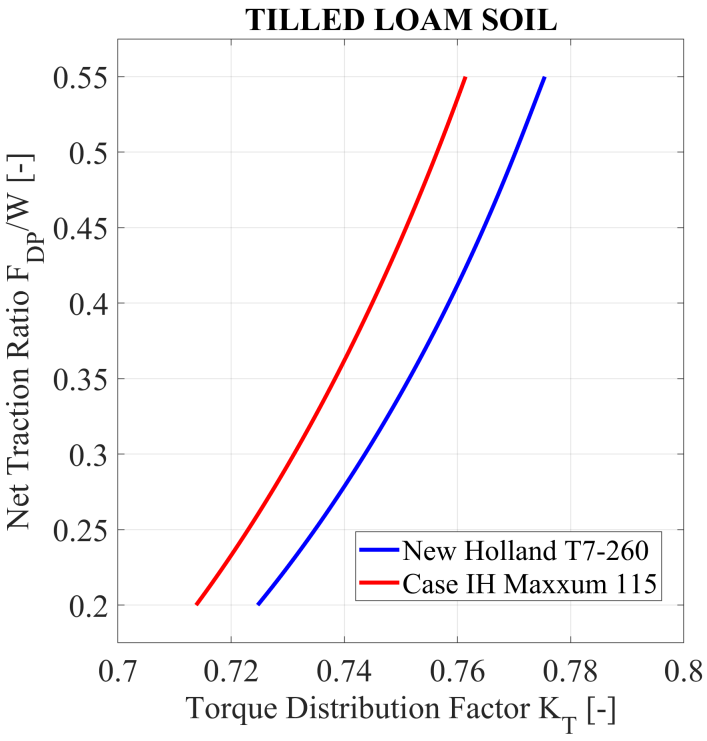

Figure 3.7: Typical trend of the torque distribution factor K_T, computed on a simulative basis

Through the analysis of Fig.3.7 is possible to understand that the torque distribution factor K_T varies not linearly with the drawbar force F_{DP} and tends to be shifted rearwards by increasing the drawbar force, however remaining within the 0.7 and 0.8 range for both the vehicles. In other words, this means that the torque delivered by the engine is distributed to the rear wheels in a rate varying between 70% and 80% of the total

[1]The Torque Distribution Factor K_T is defined as: $K_T = \frac{M_r}{M_r+M_f}$, where M_f is the torque at the front axle and M_r is the torque at the rear axle.

3.3 Gradient Method

The usage of the gradient method is aimed to exclude those constructive parameters which do not have an influence on the power delivery efficiency η_T, it relies on the analysis of the direction cosines of $\nabla\hat{\eta_S}$, $\nabla\hat{\eta_M}$ and $\nabla\hat{\eta_T}$.

From an accurate analysis of Fig. 3.8a is possible to infer that:

- The power delivery efficiency η_T is mainly influenced by three parameters: mass distribution K_M, front to rear ratio of kinetic rolling radii K_W and the lead of front wheels L.
- Observing the sign of the three most influential direction cosines of $\nabla\hat{\eta_T}$ is possible to see that K_W^* lays in the positive part of the plot denoting a monotonic increasing behavior; while K_M^* and L^* lay both in the positive and negative part of the plane showing a non-monotonic behavior, hence within the explored domain the power delivery efficiency has a maximum in these directions and the set of design parameters that maximize the power delivery efficiency is the optimal one.
- The direction cosines computed along the h^* and B^* directions remain always close to zero, emphasizing a low influence on $\hat{\eta_T}$. This fact means that even changing by far the wheelbase and the drawbar position, the power delivery efficiency remains approximately the same.

The analysis of the direction cosines of $\nabla\hat{\eta_S}$ (Fig. 3.8b) leads to the same conclusions as for $\nabla\hat{\eta_T}$; indeed for $\nabla\hat{\eta_M}$ is important to remark that just the mass distribution K_M and front to rear ratio of kinetic rolling radii K_W plays a crucial role, while the influence of L can be assumed as negligible.

3.3.1 Optimal layout of the tractor

As prevously discussed, within the explored domain, $\hat{\eta_T}$ is a monotonically increasing function of K_W and a non-monotonical function of K_M and L. The mathematical description of this behavior is entrusted to a polynomial equation which is of the first order in K_W and of the second order in K_M and L. In order to keep the mathematical formulation as simple as possible, the same function prototype was used for the regression model of $\hat{\eta_T}$, $\hat{\eta_M}$ and $\hat{\eta_S}$; the polynomial equation having the characteristics indicated is shown below (Eq. 3.1):

$$\hat{\eta_i} = \alpha_1^i + \alpha_2^i K_M + \alpha_3^i L + \alpha_4^i K_W + \alpha_5^i K_M^2 + \alpha_6^i L^2 + \alpha_7^i K_M K_W + \alpha_8^i K_M L + \alpha_9^i K_W L \quad (3.1)$$

$$\hat{\eta_i} = f(K_M, K_W, L)$$

Knowing that the generic subscript i could be $i = S, M, T$.

All the α_n coefficient indicated in the Eq.3.1 are reported in the Table 3.5:

The fitting accuracy between numerical simulations and regression surfaces, computed through the coefficient of determination R^2, is very satisfactory and the values are reported below in Table 3.6. This fact means that the regression equations can properly describe the behavior outlined by numerical simulations.

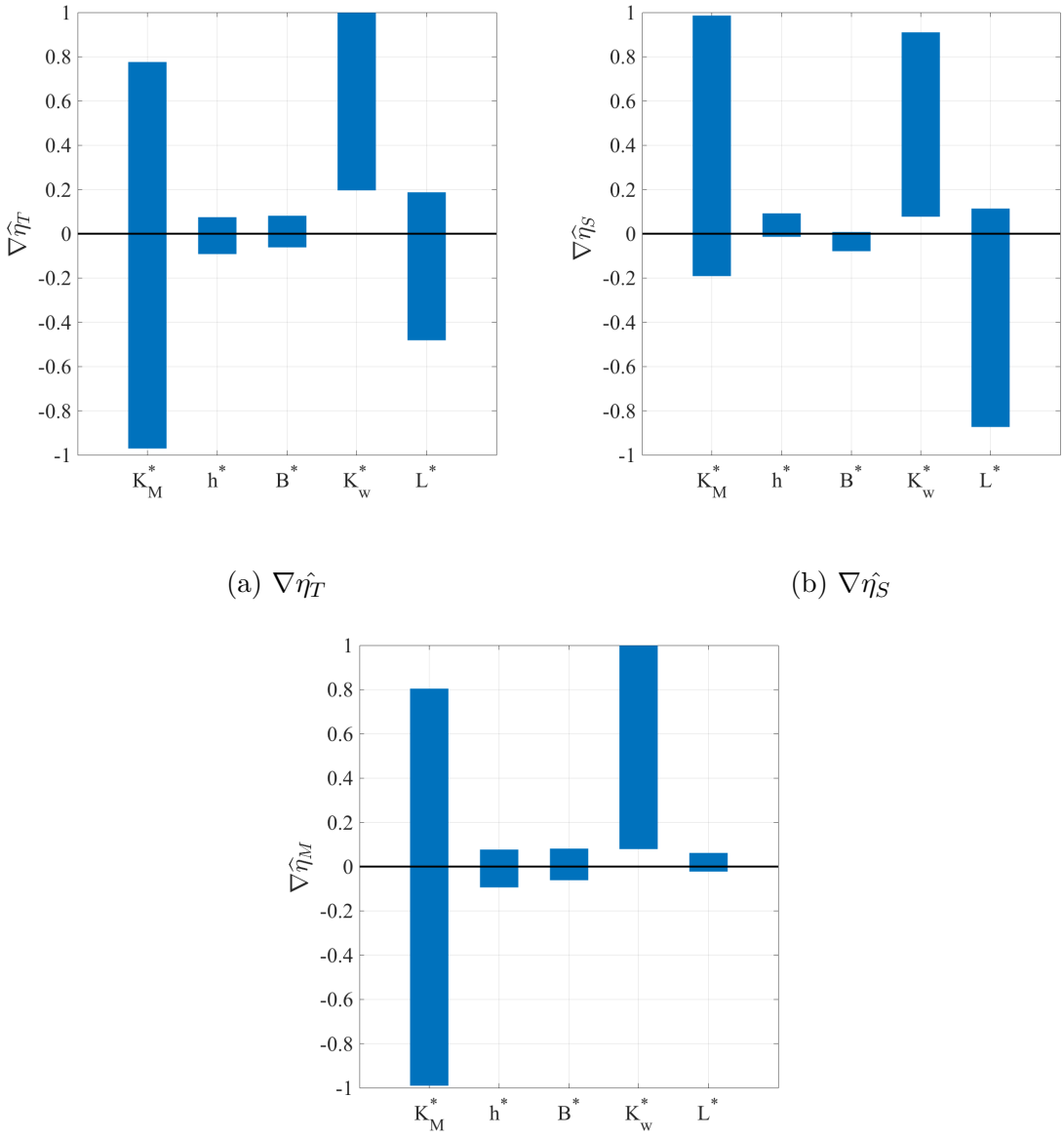

(a) $\nabla\hat{\eta}_T$

(b) $\nabla\hat{\eta}_S$

(c) $\nabla\hat{\eta}_M$

Figure 3.8: Direction cosines of the gradient of the power delivery efficiency (a), the slip efficiency (b) and the motion efficiency (c) with respect to the scaled variable parameters. Each direction cosine refers to a tractor design parameter among those under investigation. For each plot, the vertical bar encloses the values of the direction cosines of the gradient calculated for all the simulations performed.

	α_1	α_2	α_3	α_4	α_5	α_6	α_7	α_8	α_9
$\hat{\eta_T}$	0.403	0.307	−0.164	0.172	−0.114	−0.517	−0.201	0.283	−0.022
$\hat{\eta_S}$	0.834	0.034	−0.202	0.077	0.053	−0.705	−0.085	0.397	−0.077
$\hat{\eta_M}$	0.581	0.379	−0.053	0.162	−0.196	0.037	−0.194	0.031	0.043

Table 3.5: Values of the α_n coefficient concerning the efficiencies regression models

	R^2
$\hat{\eta_T}$	0.986
$\hat{\eta_S}$	0.985
$\hat{\eta_M}$	0.975

Table 3.6: Fitting accuracy of the regression surfaces

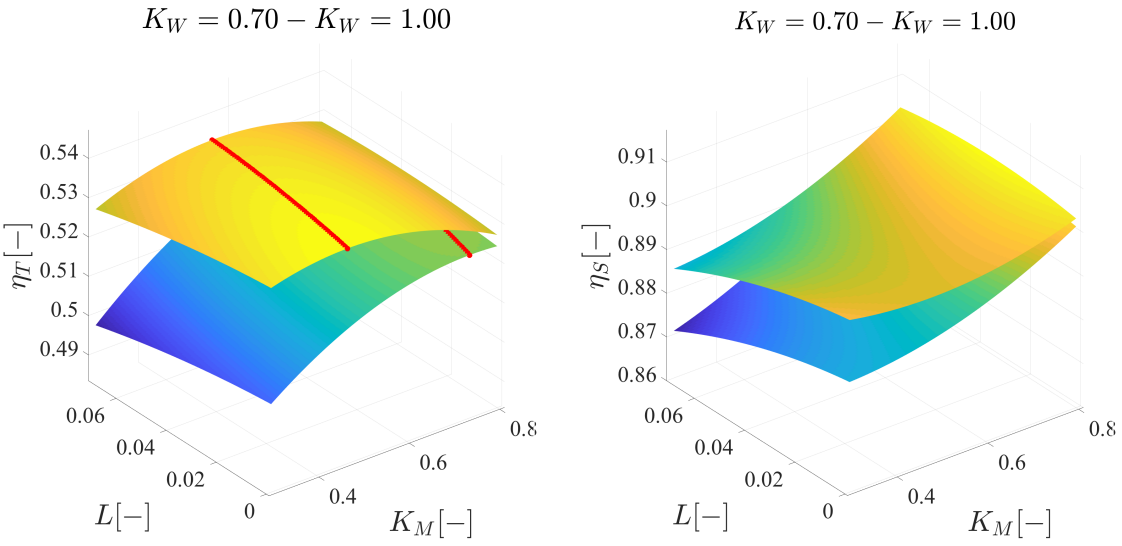

(a) $\hat{\eta_T}$

(b) $\hat{\eta_S}$

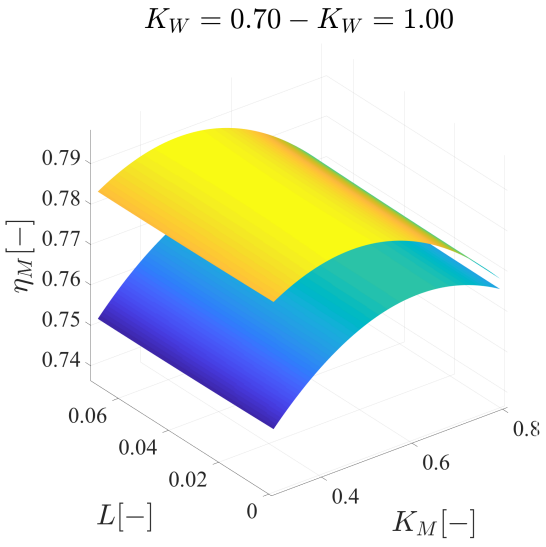

(c) $\hat{\eta_M}$

Figure 3.9: Three-dimensional representation of the influence of K_M, L and K_W on $\hat{\eta_T}$, $\hat{\eta_M}$ and on $\hat{\eta_S}$

The 3D representation of the regression surfaces (Fig. 3.9) shows that:

- The peak of the slip efficiency $\hat{\eta_S}$ is achieved when the vehicle is an iso-diametric tractor having the vast majority of mass acting on the rear axle (high value of K_M); $\hat{\eta_S}$ have a range of variation between 0.869 and 0.907 (see

Fig. 3.9b and Figs. 3.18-3.19-3.20-3.21).

- The motion efficiency $\hat{\eta_M}$ is practically independent from the lead L; furthermore, similarly to the slip efficiency $\hat{\eta_S}$, the peak is reached when the tractor is iso-diametric but with a mass distribution equally distributed between front and rear axle ($K_M \simeq 0.5$); $\hat{\eta_M}$ have a range of variation between 0.743 and 0.786 (see Fig. 3.9c and Figs. 3.14-3.15-3.16-3.17).

- The power delivery efficiency $\hat{\eta_T}$ have a range of variation between 0.549 and 0.599 (see Fig. 3.9a and Figs. 3.10-3.11-3.12-3.13) and the maximum value of the power delivery efficiency η_T is reached for a tractor having $K_W = 1$, $K_M = 0.46$ and $L = 0$.

For each tractor configuration there is an optimal mass distribution $K_{M,opt}$ that maximizes the power delivery efficiency, represented as red lines in Fig. 3.9a and in Figs. 3.10-3.11-3.12-3.13), of course this value is not fixed but depends on K_W and L and can be computed imposing the first derivative of the Eq. 3.1 equal to zero, thus leading to the following expression Eq. 3.2:

$$K_{M,opt} = \frac{-\alpha_2 - \alpha_7 \cdot K_W - \alpha_8 \cdot L}{2 \cdot \alpha_5} \tag{3.2}$$

Within the boundary of the explored domain of this thesis, $K_{M,opt}$ may vary between 0.46 and 0.8 (see Fig. 3.9a and Figs. 3.10-3.11-3.12-3.13) depending on K_W and L.

The computation of the optimal mass distribution (Eq. 3.2) translates into daily practice in the choice of the correct ballast position: isodiametric tractors, typically characterized by $K_M = 0.5$, will have greater efficiency by using a front ballast, while more traditional tractors with non-isodiametric wheels, typically characterized by $K_M = 0.6$, it would be better to ballast them directly on the rear axle.

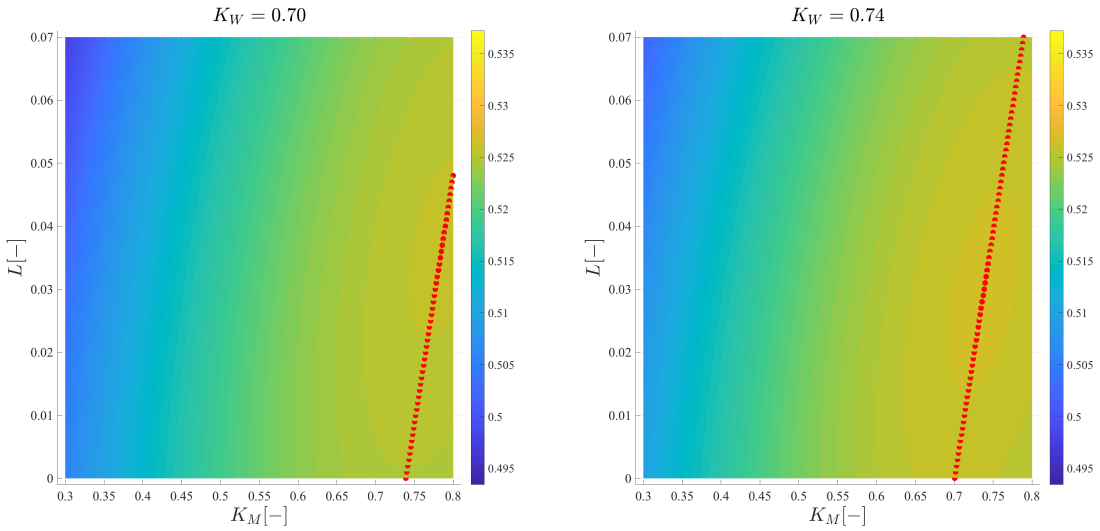

(a) $K_W = 0.70$ (b) $K_W = 0.74$

Figure 3.10: Heatmaps of the power delivery efficiency $\hat{\eta_T}$ coming from the regression equations as a function of L, K_M and K_W; the subplot on the left handside corresponds to a value of front-to-rear ratio of kinetic rolling radii K_W equal to 0.70 while the subplot on the right handside to a value of K_W equal to 0.74.

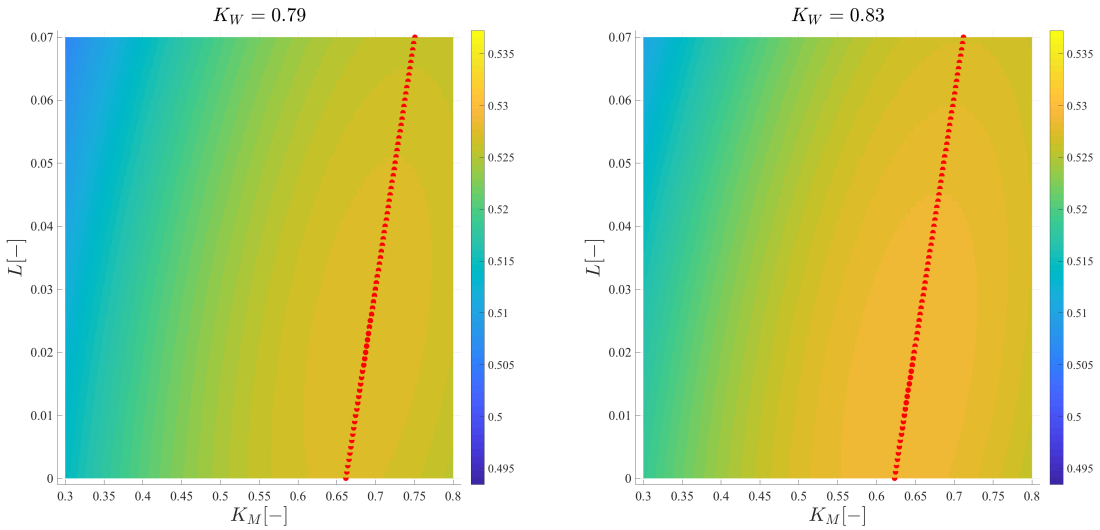

(a) $K_W = 0.79$ (b) $K_W = 0.83$

Figure 3.11: Heatmaps of the power delivery efficiency $\hat{\eta_T}$ coming from the regression equations as a function of L, K_M and K_W; the subplot on the left handside corresponds to a value of front-to-rear ratio of kinetic rolling radii K_W equal to 0.79 while the subplot on the right handside to a value of K_W equal to 0.83.

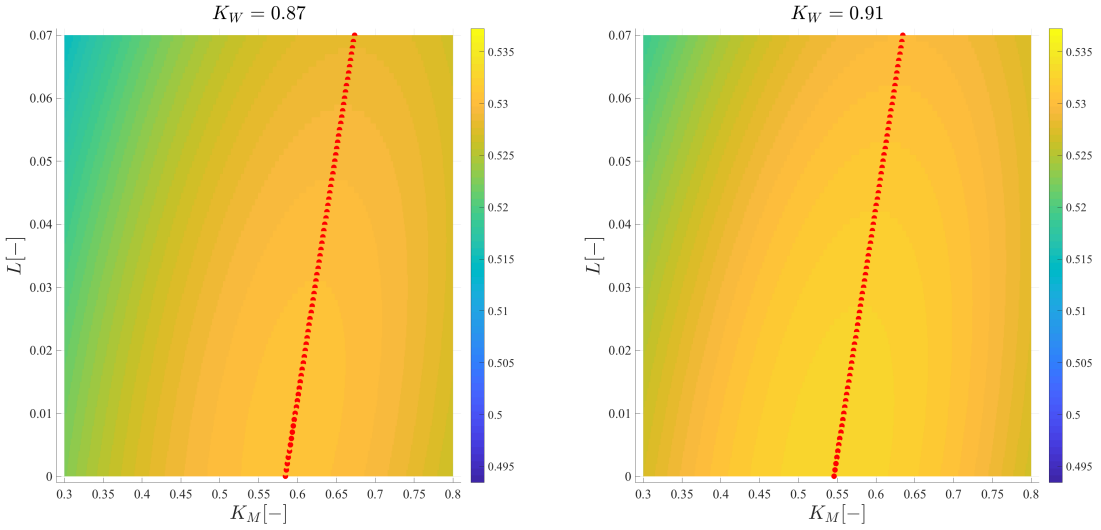

(a) $K_W = 0.87$ (b) $K_W = 0.91$

Figure 3.12: Heatmaps of the power delivery efficiency $\hat{\eta_T}$ coming from the regression equations as a function of L, K_M and K_W; the subplot on the left handside corresponds to a value of front-to-rear ratio of kinetic rolling radii K_W equal to 0.87 while the subplot on the right handside to a value of K_W equal to 0.91.

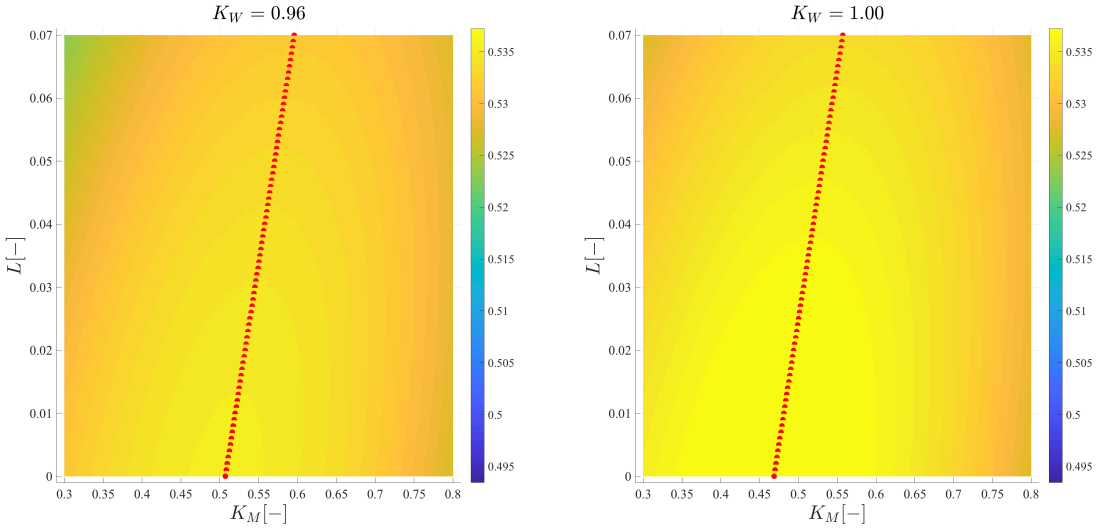

(a) $K_W = 0.96$ (b) $K_W = 1.00$

Figure 3.13: Heatmaps of the power delivery efficiency $\hat{\eta_T}$ coming from the regression equations as a function of L, K_M and K_W; the subplot on the left handside corresponds to a value of front-to-rear ratio of kinetic rolling radii K_W equal to 0.96 while the subplot on the right handside to a value of K_W equal to 1.00.

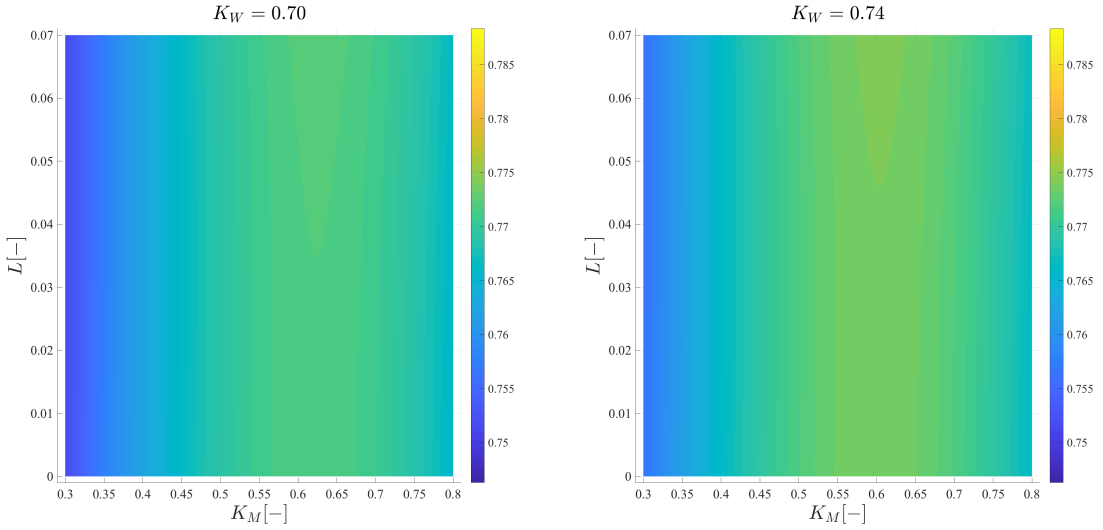

(a) $K_W = 0.70$ (b) $K_W = 0.74$

Figure 3.14: Heatmaps of the motion efficiency $\hat{\eta_M}$ coming from the regression equations as a function of L, K_M and K_W; the subplot on the left handside corresponds to a value of front-to-rear ratio of kinetic rolling radii K_W equal to 0.70 while the subplot on the right handside to a value of K_W equal to 0.74.

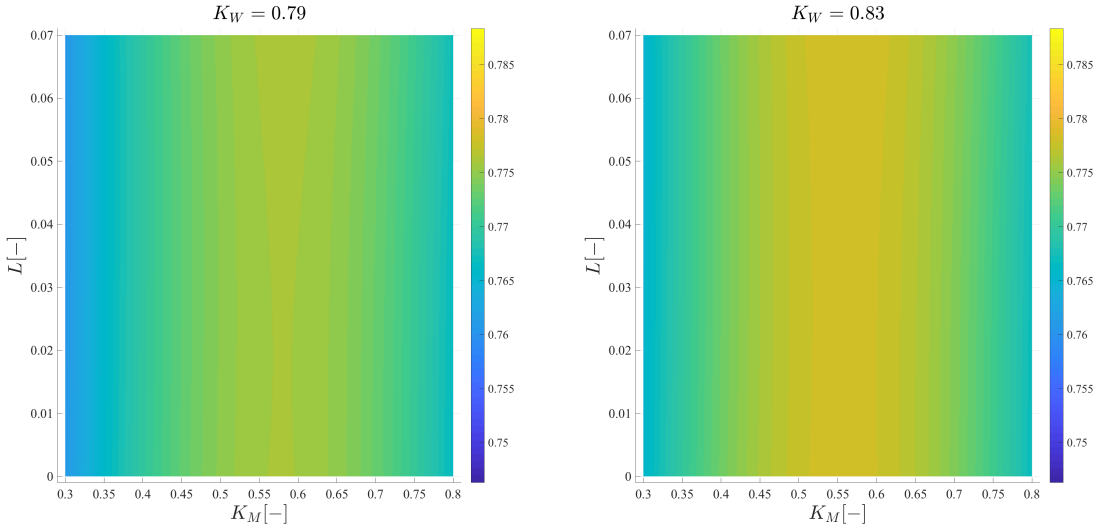

(a) $K_W = 0.79$ (b) $K_W = 0.83$

Figure 3.15: Heatmaps of the motion efficiency $\hat{\eta_M}$ coming from the regression equations as a function of L, K_M and K_W; the subplot on the left handside corresponds to a value of front-to-rear ratio of kinetic rolling radii K_W equal to 0.79 while the subplot on the right handside to a value of K_W equal to 0.83.

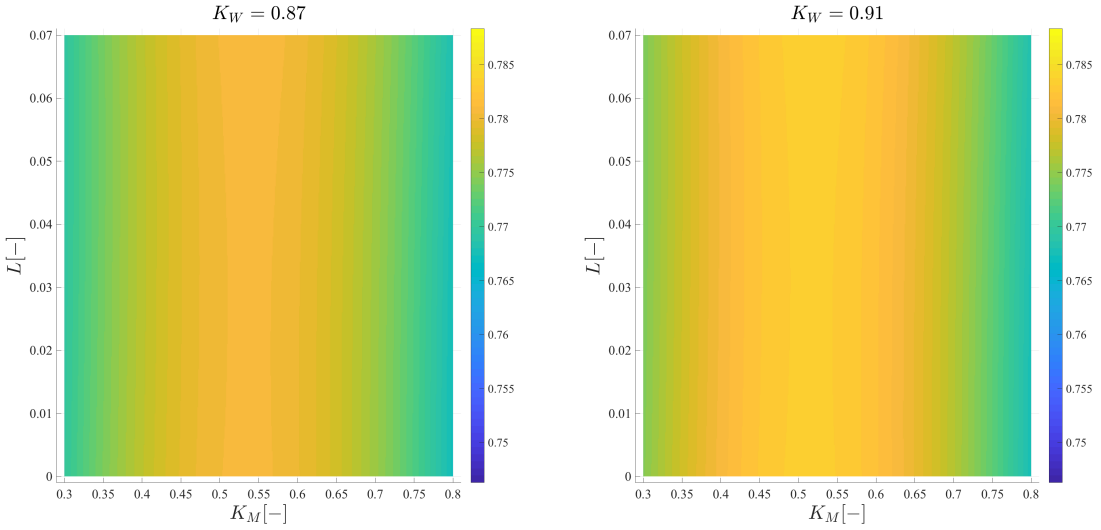

(a) $K_W = 0.87$ (b) $K_W = 0.91$

Figure 3.16: Heatmaps of the motion efficiency $\hat{\eta_M}$ coming from the regression equations as a function of L, K_M and K_W; the subplot on the left handside corresponds to a value of front-to-rear ratio of kinetic rolling radii K_W equal to 0.87 while the subplot on the right handside to a value of K_W equal to 0.91.

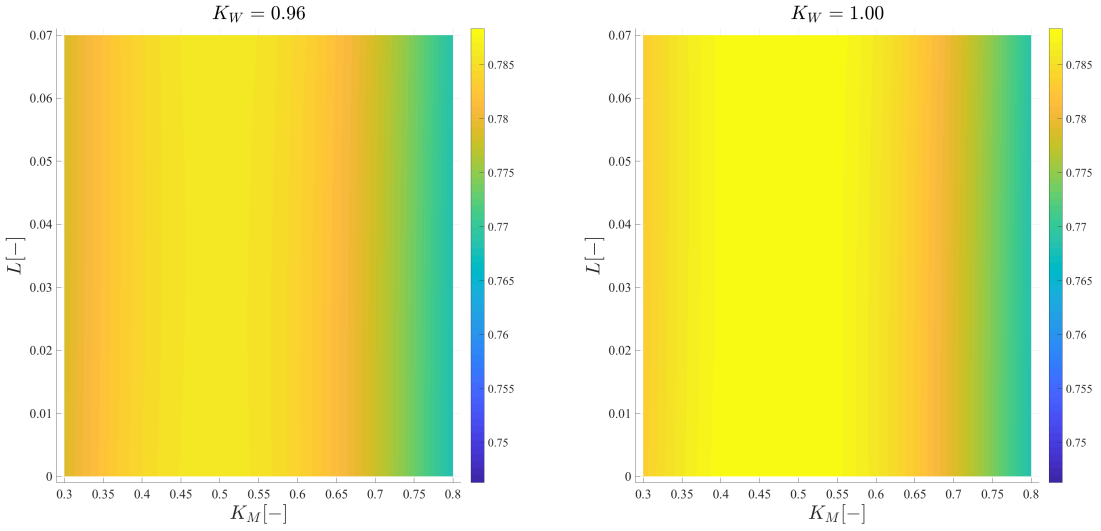

(a) $K_W = 0.96$ (b) $K_W = 1.00$

Figure 3.17: Heatmaps of the motion efficiency $\hat{\eta_M}$ coming from the regression equations as a function of L, K_M and K_W; the subplot on the left handside corresponds to a value of front-to-rear ratio of kinetic rolling radii K_W equal to 0.96 while the subplot on the right handside to a value of K_W equal to 1.00.

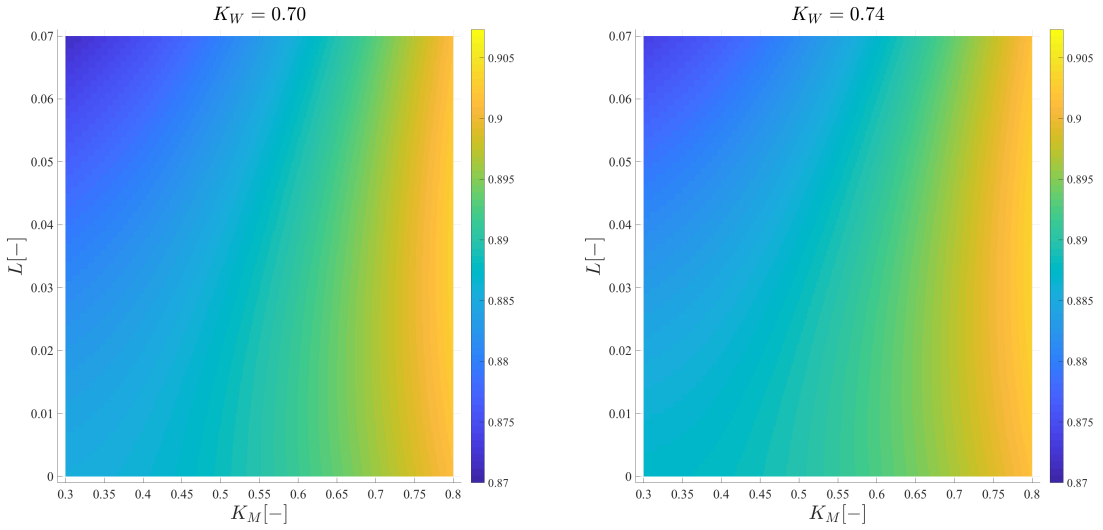

(a) $K_W = 0.70$ (b) $K_W = 0.74$

Figure 3.18: Heatmaps of the slip efficiency $\hat{\eta_S}$ coming from the regression equations as a function of L, K_M and K_W; the subplot on the left handside corresponds to a value of front-to-rear ratio of kinetic rolling radii K_W equal to 0.70 while the subplot on the right handside to a value of K_W equal to 0.74.

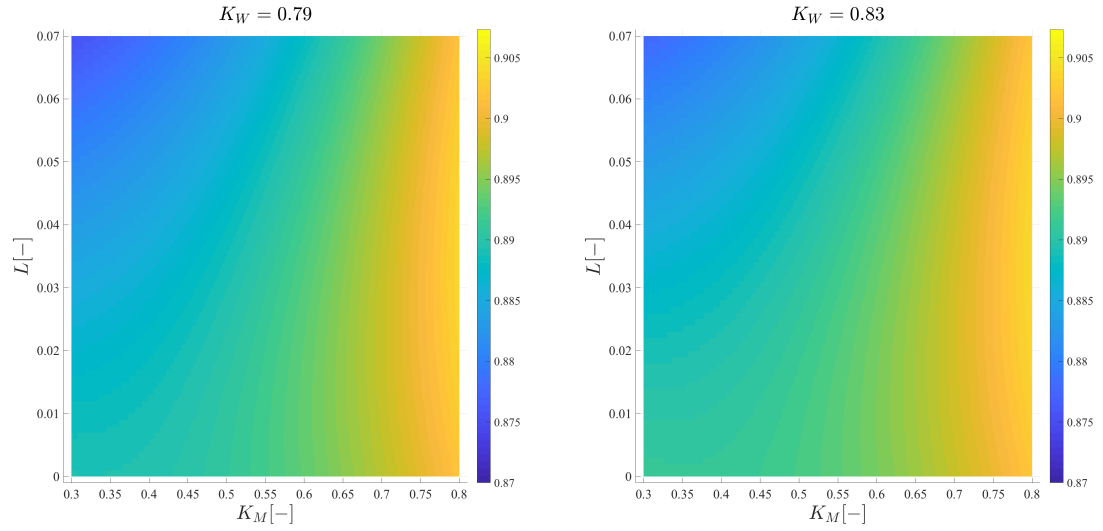

(a) $K_W = 0.79$ (b) $K_W = 0.83$

Figure 3.19: Heatmaps of the slip efficiency $\hat{\eta_S}$ coming from the regression equations as a function of L, K_M and K_W; the subplot on the left handside corresponds to a value of front-to-rear ratio of kinetic rolling radii K_W equal to 0.79 while the subplot on the right handside to a value of K_W equal to 0.83.

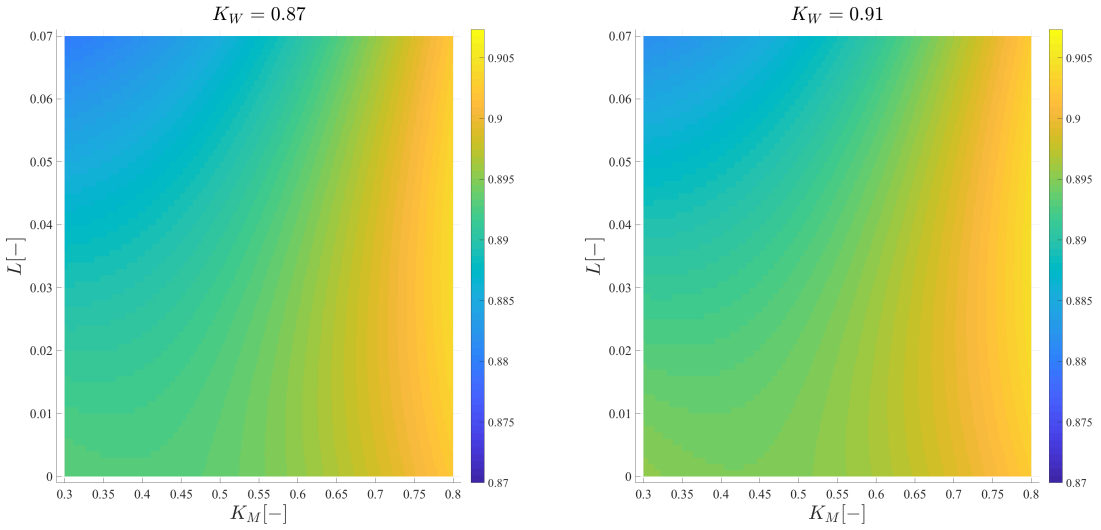

(a) $K_W = 0.87$ (b) $K_W = 0.91$

Figure 3.20: Heatmaps of the slip efficiency $\hat{\eta}_S$ coming from the regression equations as a function of L, K_M and K_W; the subplot on the left handside corresponds to a value of front-to-rear ratio of kinetic rolling radii K_W equal to 0.87 while the subplot on the right handside to a value of K_W equal to 0.91.

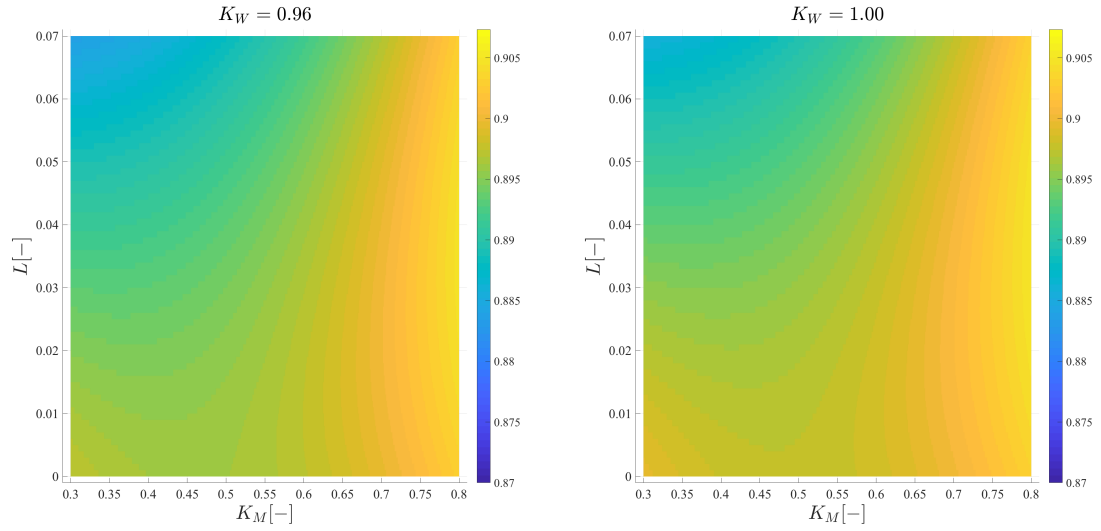

(a) $K_W = 0.96$ (b) $K_W = 1.00$

Figure 3.21: Heatmaps of the slip efficiency $\hat{\eta}_S$ coming from the regression equations as a function of L, K_M and K_W; the subplot on the left handside corresponds to a value of front-to-rear ratio of kinetic rolling radii K_W equal to 0.96 while the subplot on the right handside to a value of K_W equal to 1.00.

Chapter 4

Conclusions

The main goal of this study was to understand which are the most influential constructive parameters on the power delivery efficiency of a mechanical front wheel drive (M.F.W.D.) agricultural tractor. For the development of this study an analytical-modeling approach was chosen since allows to overcome the typical experimental constraints, such as the fact that is difficult to have many tractors to test with just one different constructive feature, the development of a model allows to a vary the parameters independently from one another and inside a wide range of variation.
The model described in this study has reached an excellent level of completeness and comprehension of the mechanics underlying at the wheel-soil interface but could be further expanded by inserting all the variables that can be governed by the driver, such as the inflation pressure of the tires. The model proposed was quite complex thus an experimental validation had been carried out using a row-crop tractor running on different soil conditions (tilled clayey loam, tilled loam, untilled loam) and with different mass distributions, the fitting between experimental and simulated data was satisfactory and the shape of the power delivery efficiency curve as a function of drawbar pull and of vehicle slip was consistent with the technical literature and with the measurements.
A gradient-based method was helpful in the comprehension of which are the top three most influential constructive parameters, among those studied (static mass distribution, wheelbase, front to rear ratio of kinetic rolling radii, lead of the front wheels and drawbar location), the most influential constructive features are the static mass distribution K_M, the front-to-rear ratio of kinetic rolling radii K_W and the lead of the front wheels L.
Within the boundary of the explored domain appears that the tractor configuration which maximizes the power delivery efficiency is a vehicle having no lead on the front wheels, isodiametric wheels and the majority of the static mass distribution acting on the front axle (54% acting on the front axle and 46% acting on the rear axle), moreover the optimal static mass distribution is not constant but can vary a lot depending on the values of front to rear ratio of kinetic rolling radii K_W and of the front wheels lead L; is necessary also to clarify that the choice of K_W and L, typically made by the manufacturer, is not solely based on the power delivery efficiency or tractive performances but also on steering kinematics, driveability and comfort.
From the simulations performed and looking at the regression surfaces clearly appears that if the front-to-rear ratio of kinetic rolling radii decreases also the power delivery efficiency decreases; moreover if the lead of the front wheels increases the

optimal mass distribution tends to be shifted rearwards, this is a consequence of the fact that the front wheels lead enforce the front axle to have a much greater wheel slip than the rear axle.
For a generic non-isodiametric row crop tractor having the front-to-rear ratio of kinetic rolling radii K_W equal to 0.7 and front wheels lead L equal to 0.03, which is a quite common tractor's layout, exhibits an optimal mass distribution subdivided in 76% on the rear axle and 24% on the front axle. In conclusion, from this thesis it can be drawn that the parameters which affect the power delivery efficiency are multiple and strictly correlated to one-another; in this framework, a model able to predict the efficiency of the vehicle can be a very interesting tool. Furthermore, understanding how the constructive characteristics of the tractor affect the optimal mass distribution can give useful suggestions, especially in the ballasting phase, transforming this study into something applicable in the everyday practice.

Bibliography

[1] Aubel, T. (1993). FEM simulation of the interaction between an elastic tire and soft soil. Proc 10th Intl. Conf. ISTVS, 791-802.

[2] Baladi, G. Y., and B. Rohani. (1984). Development of a soil-wheel interaction model. Proc 8th Intl. Conf. ISTVS, 33-59.

[3] Bashford, L. L., K. Von Bargen, T. R. Way, and L. Xiaoxian. (1987). Performance comparisons between duals and singles on rear axles of a front wheel assist tractor. Trans. ASAE 30(3):641-645.

[4] Bekker, M. G. (1956). Theory of Land Locomotion: The Mechanics of Vehicle Mobility. Ann Arbor, Mich.: Univ. Michigan Press.

[5] Bekker, M. G. (1969). Introduction to terrain-vehicle systems. Ann Arbor, MI: University of Michigan Press.

[6] Brixius, W. W. (1987). Traction prediction equations for bias ply tires. ASAE Paper No. 87-1622. St. Joseph, Mich.: ASAE.

[7] Byerly, D. V., L. L. Bashford, R. D. Grisso, and K. Von Bargen. (1989). Tractive performance and fuel consumption of a 2WD tractor. SAE Paper No. 89-1837. Warrendale, Pa.: SAE.

[8] Charles, M., and D. J. Schuring. (1984). An empirical model for predicting the effective rolling radius of agricultural drive tires. ASAE Paper No. 84-1555 St. Joseph, Mich.: ASAE.

[9] Evans, M. D., R. L. Clark, and G. Manor. (1989). A traction prediction and ballast selection model. ASAE Paper No. 89-1054. St. Joseph, Mich.: ASAE.

[10] Evans, M. D., R. L. Clark, and G. Manor. (1991). An improved traction model for ballast selection. Trans. ASAE 34(3): 773-780.

[11] Fervers, C. W. (2004). Improved FEM simulation model for tire-soil simulation. Journal of Terramechanics 41:87-100.

[12] Freitag, D. R. (1966). A dimensional analysis of the performance of pneumatic tires on clay. Journal of Terramechanics 3: 51-68.

[13] Fujimoto, Y. (1977). Performance of elastic wheels on yielding cohesive soils. Journal of Terramechanics, 14(4), 191-210.

[14] Goering, C. E. (1992). Engine and tractor power (3rd ed.). St. Joseph, MI: American Society of Agricultural Engineers (ASAE).

[15] Harris, H. D.; Pearce, F. (1990). A universal mathematical model of diesel engine performance. Journal of Agricultural Engineering Research, 47: 165-176.

[16] Harris, H. D. (1992). Prediction of the torque and optimum operating point of diesel engines using engine speed and fuel consumption. Journal of Agricultural Engineering Research, 47: 165-176.

[17] Ibuki, T., and A. Oida (2000). Simulation to analyze the interaction between soil and a tire lug by distinct element method. Proc. 8th European ISTVS Conf. 87-93

[18] Jahns, G., (1983). A method of describing diesel engine performance maps. ASAE Paper NCR 83-103. ASAE, St Joseph, MI.

[19] Janosi, Z., Hanamoto, B. (1961). The analytical determination of drawbar pull as a function of slip for tracked vehicles in deformable soils. Proc. of ISTVS Turin (p. 1961).

[20] Janulevicius, A., Damanauskas, V., & Pupinis, G. (2018). Effect of variations in front wheels driving lead on performance of a farm tractor with mechanical front-wheel drive. Journal of Terramechanics, 77, 23-30.

[21] Janulevicius, A., Pupinis, G., Lukstas, J. Damanauskas, V., & Kurkauskas, V. (2017). Dependencies of the lead of front driving wheels on different tire deformations for a MFWD tractor. Transport, 32(1), 23-31.

[22] Kiss, P. (2003). Rolling radii of pneumatic tyre on deformable soil. Biosystems Engineering, 85(2), 153-161.

[23] Liang, Z., Gao, H., Ding, L., Deng, Z., & Qu, J. (2014). Analysis of driving efficiency for LRV wheels using forced-slip method. Advances in Space Research, 54(10), 2122-2130.

[24] Nakashima, H., and A. Oida. (2004). Algorithm and implementation of soil-tire contact analysis code based on dynamic FE-DE method. Journal of Terramechanics 41: 127-137

[25] Perdok, U. D. (1978). A prediction model for the selection of tyres for towed vehicles on tilled soil. Journal of Agricultural Engineering Research, 23(4), 369-383.

[26] Regazzi, N., Maraldi, M., Molari, G., (2019). A theoretical study of the parameters affecting the power delivery efficiency of an agricultural tractor. Biosys-

tems Engineering, 186, 214-227.

[27] Schmid, I. C. (1995). Interaction of vehicle and terrain results from 10 years research at IKK. Journal of Terramechanics 32(1): 3-26.

[28] Schreiber, M. (2012) Kraftstoffverbrauch beim Einsatz von Ackerschleppern im besonderen Hinblick auf die CO_2 Emissionen (Doctoral thesis). Stuttgart, Germany, Universitaet Hohenheim.

[29] Senatore, C., & Sandu, C., (2011, a). Off-road tire modeling and the multi-pass effect for vehicle dynamics simulation. Journal of Terramechanics, 48(4), 265-276.

[30] Senatore, C., & Sandu, C., (2011, b). Torque distribution influence on tractive efficiency and mobility of off-road wheeled vehicles. Journal of Terramechanics, 48(5), 372-383.

[31] Stoilov, S., & Kostadinov, G. D. (2009). Effect of weight distribution on the slip efficiency of a four wheel drive skidder. Biosystems Engineering, 104(4), 486-492.

[32] Turnage, G. W. 1972. Tire selection and performance prediction for off-road wheeled vehicle operations. Proc. 4th Intl. Conf. ISTVS, 1: 61.

[33] Upadhayaya, S. K., U. A. Rosa, and D. Wulfsohn. (2002). Application of the finite element method in agricultural soil mechanics. Advances in Soil Dynamics, 2: 117-153.

[34] Upadhyaya S. K., W. J. Chancellor, J. V. Perumpral, D. Wulfsohn, and T. R. Way, (2009). Advances in Soil Dynamics Volume 3. eds. St. Joseph, Mich.: American Society of Agricultural and Biological Engineers.

[35] Upadhyaya, S. K., D. Wulfsohn, and J. Mehlschau. (1993). An instrumented device to obtain traction related parameters. Journal of Terramechanics 30(1):1-20.

[36] Wismer, R. D., and H. J. Luth. (1973). Off-road traction prediction for wheeled vehicles. Journal of Terramechanics 10: 49-61.

[37] Wismer, R. D., and H. J. Luth. (1973). Off-road traction prediction for wheeled vehicles. Trans. ASAE 17(1): 8-10, 14.

[38] Wang, G., (1988). A Microprocessor-based analysis of tractor performance. Ph.D. thesis. Saskatoon, Sask., Canada: University of Saskatchewan.

[39] Wang, G., Zoerb, G. C. (1989). Determination of optimum working points for diesel engines. Journal of the ASAE, 25: 1519-1522.

[40] Wong, J. Y. (1989). Terramechanics and off-road vehicles. Amsterdam: Elsevier.

[41] Wong, J. Y. (2010). Terramechanics and off-road vehicle engineering (2nd ed.). Amsterdam: Elsevier.

[42] Wong, J.Y., & Reece, A. R. (1967 a). Prediction of rigid wheel performance based on the analysis of soil-wheel stresses, Part I. Performance of driven rigid wheels. Journal of Terramechanics, 4(1), 81-98.

[43] Wong, J.Y., & Reece, A. R. (1967 b). Prediction of rigid wheel performance based on the analysis of soil-wheel stresses, Part II. Performance of towed rigid wheels. Journal of Terramechanics, 4(2), 7-25.

[44] Zoz, F. M., and W. W. Brixius. (1979). Traction prediction for agricultural tires on concrete. ASAE Paper No. 79-1046. St. Joseph, Mich.: ASAE.